FACULTAD DE FÍSICA
PONTIFICIA UNIVERSIDAD
CATÓLICA DE CHILE

Long lived Heavy Neutral Leptons from Z’ decays at the FCC-ee

by

Mariel Luz Poduje Reyes

Thesis submitted to the Faculty of Physics
of Pontificia Universidad Católica de Chile, as one of the requirements
to qualify for the academic Master’s degree in Physics.

Supervisor : Dr. Giovanna Cottin
Co-Supervisor : Dr. Francisca Garay
Committee : Dr. Marco Aurelio Díaz

Santiago, Chile
January, 2025

To my beloved family and friends

Abstract

We study the phenomenology of a $U(1)_{B-L}$ extension of the Standard Model (SM) predicting long-lived heavy neutral leptons (HNLs), which are pair produced from a new gauge boson Z' with displaced vertex signatures at the electron positron mode of the Future Circular Collider (FCC-ee). Progress on sensitivity prospects are provided in the 1-100GeV mass scale for the B-L gauge coupling $g' = 10^{-3}$ and 10^{-4}, and HNL-light neutrino mixing $|V_{\mu N}|^2 = 10^{-8} - 10^{-20}$, a region that has not been constrained by the Large Hadron Collider (LHC). Exclusion curves are obtained for a configuration of the IDEA detector with and without a LAYCAST-like far detector on the HNL vs Z' mass plane ($M_N - M_{Z'}$) and the HNL mass vs heavy-light squared neutrino mixing plane ($M_N - |V_{\mu N}|^2$).

Acknowledgements

I would like to thank my advisors, Giovanna Cottin and Francisca Garay, for their time and patience dedicated to the development of this work. I am also grateful to Bruno Zerega for his companionship throughout our venture into long-lived heavy neutrinos. Additionally, I thank Giovanna, Francisca, and Marco Aurelio Diaz for all of the support they have given me through recommendation letters.

This work received finantial support from ANID Fondecyt grant number 11220237 and 1240721. ANID-Subdirección de Capital Humano/Magíster Nacional/2024 - 22241306

Contents

List of Figures

List of Tables

Chapter 1

Introduction

1.1 The Standard Model and it's shortcomings

The Standard Model (SM) of particle physics is a quantum field theory that predicts the existence of fermionic elementary particles that can interact with each other. These particles compose a part of the mass content of the universe[1]. The model also predicts that the interactions between them are mediated by bosonic elementary particles and are identified as the carriers for three of the four forces of nature: electromagnetic, strong and weak forces. The fermionic particles are divided in two groups, the leptons and quarks, and they exist in three generations with different masses and names. In the SM, particles get a mass through the only scalar boson of the theory, the Higgs boson, whose associated field, with which particles interact, acquires a expectation value in vacuum, v, spontaneously breaking the Electro-Weak (EW) symmetry.

The fact that the SM is a quantum field theory means that particles can be described by fields in a Lagrangian, and that such fields are quantized. The different sectors of the theory

---

[1] Actually, the particles of the SM, so-called barionic matter, is known to compose only 5% of the mass-energy of the universe, the other 68% and 27% corresponding to the dark energy and dark matter of the universe, respectively [1].

correspond to each type of interaction and have qualities that are dictated by different gauge symmetries. The full gauge symmetry of the model correspond to the $U(1)_Y \times SU(2)_L \times SU(3)_C$ group, which conserves three corresponding gauge charges: the hypercharge Y, the third component of isospin, T_3, and the color charge, C. Another relevant theoretical property is that the Standard Model is also a renormalizable quantum field theory. This means that any divergence resulting from the calculations of physical quantities within the framework can be absorbed into a redefinition of a finite set of free parameters (e.g., masses, couplings, and field normalizations). As a result, the theory yields finite predictions for observable quantities. After the theory is renormalized, the parameters of the model become dependent on the energy scale according to the renormalization group evolution. A complete theoretical insight on renormalizable quantum field theories is provided in reference [2].

The gauge group corresponding to the EW symmetry is $U(1)_Y \times SU(2)_L$, and the full covariant derivative of the SM is

$$D_\mu = \partial_\mu + ig_s \mathcal{T}_\alpha G^\alpha_\mu + igT_a W^a_\mu + ig_1 Y B_\mu, \tag{1.1}$$

where g_s and g and g_1 are the $SU(3)$, $SU(2)$ and $U(1)$ gauge couplings, respectively. Y, the hypercharge, is defined as $Y = Q - T_3$, the electric charge minus the third component of the weak isospin, $T_a = \sigma_a/2$ and $\mathcal{T}_\alpha = \lambda_\alpha/2$ are the generators of the $SU(2)$ and $SU(3)$ groups, written in terms of the Pauli and Gell-Mann matrices respectively.

After EW symmetry breaking by the the VEV of the Higgs doublet,

$$\langle H \rangle = \frac{1}{\sqrt{2}} \begin{pmatrix} 0 \\ v \end{pmatrix} \tag{1.2}$$

the kinetic terms in the Lagrangian, $(D_\mu H)^\dagger (D^\mu H)$, result in two massive W bosons, W^+

and W^-, which are a combination of the gauge fields W_1^μ and W_2^μ. In the same scalar kinetic terms, the neutral component of the $SU(2)$ field, W_3^μ, mixes with the gauge field corresponding to the $U(1)$ symmetry, B_μ, forming the mass eigen states Z_μ and A_μ, and diagonalizing the mass matrix as

$$\frac{1}{8}v^2 \begin{pmatrix} A_\mu & Z_\mu \end{pmatrix} \begin{pmatrix} 0 & 0 \\ 0 & g_{\mathrm{W}}^2 + g'^2 \end{pmatrix} \begin{pmatrix} A^\mu \\ Z^\mu \end{pmatrix} \tag{1.3}$$

which results in

$$m_A = 0 \quad \text{and} \quad m_{\mathrm{Z}} = \frac{1}{2}v\sqrt{g_{\mathrm{W}}^2 + g'^2} \tag{1.4}$$

for the photon and the Z boson respectively.

The fermions in the Standard Model also gain a mass through EW symmetry breaking. This occurs by introducing terms in the Lagrangian where the scalar field interacts with the fermions, known as Yukawa interactions. These terms are invariant under the $U(1)_Y \times SU(2)_L$ symmetry group, and for leptons, they are expressed as

$$\mathcal{L}_Y \supset -y_{1k}^D \bar{l}_{1L} e_R \tilde{H}. \tag{1.5}$$

In this equation, l_{jL} is a $SU(2)$ doublet with left-handed chirality (LH) and e_R is a $SU(2)$ singlet with right-handed chirality (RH). The generation index j was fixed at 1 and therefore the RH field corresponds to a RH electron. See Table (1.1) for the complete field content of the model.

It's important to note that this model does not predict the value of the masses for each particle, instead, they are free parameters that have been measured by a variety of experiments. Some of these include the Stanford Linear Accelerator Center (SLAC), the Tevatron at Fermilab, the Large Electron-Positron Collider (LEP), the Large Hadron Collider (LHC) and others. These experiments measured most of the known masses, and we highlight the

Higgs mass, 125.1 GeV, or the Z boson mass, 91.1 GeV, which are significantly larger compared the the muon mass of 0.101 GeV, see [3–6] for a reference to each experiment and the respective measurements.

Fields	Field Content	$SU(3)_C$	$SU(2)_L$	$U(1)_Y$
g^{α}_{μ}	g^{α}_{μ}	8	1	0
$W^{\mu a}$	W^{a}_{μ}	1	3	0
B^{μ}	B^{μ}	1	1	0
L_i	L_i=$\begin{pmatrix} N_{L_i} \\ e_{L_i} \end{pmatrix}$	1	2	1/2
ℓ^{c}_{Li}	e_{R_i}	1	1	1
Q_i	$\begin{pmatrix} u_{L_i} \\ d_{L_i} \end{pmatrix}$	3	2	1/6
d^{c}_{Li}	u_{R_i}	3	1	1/3
u^{c}_{Li}	u_{R_i}	3	1	-1/3
H	$\begin{pmatrix} H^{+} \\ H^{0} \end{pmatrix}$	1	2	-1/2

Table 1.1: Standard Model of particle physics. $i = 1, ..., 3$ are generation indices, $a = 1, ..., 3$ for W and $\alpha = 1, ..., 8$ for the gluons are the group generator indices.

There are many reasons why the SM cannot be considered complete. One of it is main problems relates to the mass of one of the lepton particles, the neutrino. By construction, no mass term is included for neutrinos in the formulation of the model. This was well accepted by experimental data, since they are interpreted as missing energy in collider experiments. Another reason why a Dirac mass term analogous to those of other fermions in the Yukawa terms in equation (1.5) wasn't motivated for neutrinos is that neutrinos of right handed chirality have never been measured experimentally, therefore in the SM neutrinos are only left handed fields.

Years of collaborative efforts passed, and finally the experimental confirmation of neutrino oscillations in 1998 was able to explain the solar [7] [8] [9], atmospheric [10] and reactor neutrino anomalies [11], stating that neutrinos could oscillate from a flavor to another with a probability that is proportional to the squared mass difference between them. Therefore, neutrinos must have a mass term and the Standard Model must be extended to account for it. In the present day, it is known that neutrinos manifest as missing energy in experiments because they have an extremely small mass, making them effectively invisible to detection in particle detectors.

In this work we motivate neutrino masses via the Seesaw type I model [12] through the mixing of SM neutrinos with heavy Majorana neutrinos, so-called Heavy Neutral Leptons (HNLs). These are often called "right-handed" neutrinos due to their chirality, and in Seesaw type I they are required to be at least around two orders of magnitude bigger than the SM neutrino mass, which is estimated to be $1eV$[13], to account for it is smallness. In this work, however, we perform an analysis without taking neutrino oscillation data into consideration, because light and heavy neutrino masses are decoupled, thus the HNL mass is scanned as a free parameter with the purpose of characterizing a displaced signal for HNLs in the GeV scale.

1.2 Long-lived particles and Heavy Neutral Leptons

In the Standard Model, the particles lifetimes range from very promptly decaying particles like the Z boson or the top quark ($\tau \sim 10^{-25}$ s) to stable particles like the electron, the proton or the neutrinos. These last are examples of Standard Model long lived particles (LLPs), and their stability is, in some cases, due to the absence of decay modes within the Standard Model framework because of conserved or approximately conserved symmetries.

LLPs do not have to be fully stable particles, though, and in general they are classified as such by the signatures they can leave in particle detectors. A very relevant sign of a LLP is a trace that begins further away from the mother particle (the LLP) production point, leaving a signature called a displaced vertex (DV). Such displacement, i.e the decay length of the LLP, can be macroscopically detected starting on around the mm scale [14].

LLPs are a compelling feature of many Beyond the Standard Model (BSM) theories that aim to address some of the most fundamental questions in particle physics, such as the nature of dark matter, the hierarchy problem, baryogenesis and, as a motivation for this work, the nature of neutrino masses [15]. The existence of LLPs represents a paradigm shift in the search for new physics, extending traditional methodologies to encompass phenomena with intrinsically diverse temporal and spatial scales. If the lifetimes of the SM particles span numerous orders of magnitude, our experiments should search accordingly for BSM physics.

The reason why particle lifetimes can be long is because they may interact weakly with the Standard Model particles, or their decay processes can be suppressed due to limited phase space availability. Prominent searches for BSM LLPs in recent decades have included the charginos in supersymmetric models [16][17] and HNLs in Seesaw mechanism models [18], which will be the focus of our work. HNLs are great LLP candidates because they can couple feebly to the SM and because their decay can be mediated by an off-shell W boson, which suppresses the decay channel and leads to a small decay width bellow 10^{-13} GeV, resulting in a long lived HNL.

HNLs can be included through models like the minimal HNL model [12], where the SM gauge group is unchanged and the Seesaw mechanism include three HNLs. A more extended model is the $U(1)_X$, where X is a general quantum number associated with a new $U(1)_X$ gauge symmetry. In the case studied here, this quantum number is given by $X = B - L$, baryon minus lepton number, thus it is a particular case called the "B-L model" [19]. A more general quantum number like X allows for bigger production rates [20][21], but the B-L model can be advantageous when connecting to experimental data, since it is simpler in the assignment of quantum numbers. The B-L extension of the SM contains, besides the right handed HNLs, a new gauge boson Z' and a new scalar field χ, which breaks the $U(1)_{B-L}$ symmetry and give masses to HNLs, along with the physical gauge bosons, Z' and Z, after EW symmetry breaking. Also, as mentioned above, the HNL can decay to SM particles through the heavy-light neutrino mixing matrix $|V_{\ell N}|$, where N is the HNL and $\ell = e$, μ or τ, for the lepton generations.

Since the experimental discovery of the Higgs boson [3], no new elementary particle has been found in any collider experiment around the world. This has lead the community to wonder wether the searches done to this point have been enough at covering the whole range of hypotetical particles and how could experiments improve to detect them. Particularly, the study of particles that do not decay promptly has raised a lot of attention in recent years, not only because most LHC experiments are not built to detect anything beyond the $\mathcal{O}(10)$ m, but because long lived particles that still decay in the tracker of a detector like CMS or ATLAS could produce a DV that the hardware and data processing is not always properly optimized for detecting [14].

1.3 The B-L model at the FCC-ee

We will work on the so-called "pure" or "minimal" B-L, where tree level mixing with SM gauge bosons is null at the EW scale, and we will consider a simplified model with only one HNL, N_2, which will only mix with muon type neutrinos through the mixing matrix $|V_{\mu N}|$. Since our model is provided with an extra $U(1)$ gauge symmetry, it allows for a new production channel of two HNLs through the Z' boson. Models like this one can test the limitations of collaborations such as the LHC, as HNLs are allowed to interact very weakly with SM particles and very high-precision measurements may be required to detect such signals. This is why we focus our analysis on the high-luminosity CERN proposal, the Future Circular Collider at electron positron mode (FCC-ee). Overall, this thesis motivates the search for long lived particles at a project that aims to look for BSM physics beyond the LHC reach.

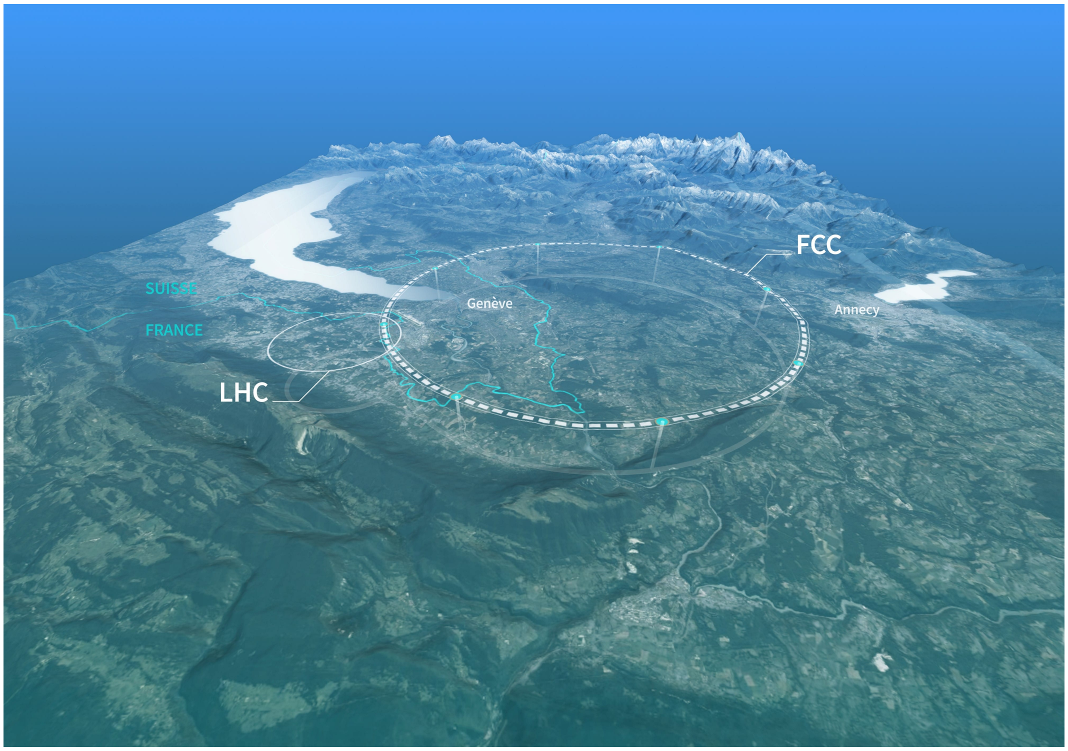

Figure 1.1: Map of the proposed location for the Future Circular Collider, [22]

In 2013, The European Strategy for Particle Physics (ESPP) stated that "To stay at the forefront of particle physics, Europe needs to be in a position to propose an ambitious post-LHC accelerator project at CERN by the time of the next Strategy update" [23]. Along with that, the scientific potential of a new electron-positron collider was highlighted as necessary to study the Higgs sector, among others, with high precision. The Future Circular Collider is the resulting proposal by CERN, and in 2020 it was highlighted as of primary importance by the ESPP again, in the 2020 update [24]. The FCC-ee is to be located on the French-Swiss border as an extension of the existing CERN infrastructure, see Figure (1.1), and it will be on feasibility studies until 2025. A key part of this process involves collaborations conducting BSM prospect studies like the one in this thesis. We propose a search for the experiment to test an unconstrained region of the B-L parameter space, which is particularly relevant because it predicts long-lived HNLs and, of course, it could be a step forward to solve the neutrino mass problem. By performing these analyses, it becomes possible to predict which BSM models can the collider put to test.

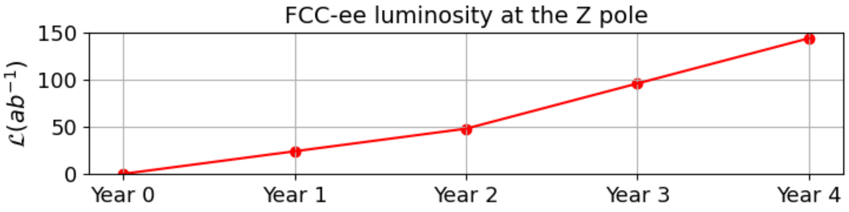

Figure 1.2: Luminosities at the Z pole at the FCC-ee. [25]

This collider is proposed to run at electron-positron mode (FCC-ee) and aims to cover up to 70TeV in center of mass energy ($\sqrt{s}$). Although not explored in this work, FCC aims to reach up to 100 TeV energy scale on it is hadron-hadron mode. The proposal consists of a 100km circumference double ring collider that is planned to run in four stages ($\sqrt{s}$,years):

Z pole (91 GeV, 4 y)$\rightarrow$ WW threshold (161 GeV, 2 y)$\rightarrow$ Higgs factory (240 GeV, 3 y)
$\rightarrow$ shutdown (1 y) $\rightarrow$ top pair threshold, (340-365GeV, 5 y)

Overall, FCC-ee would look thoroughly into the EW and Higgs sector, since it's expected to reach 10^5 times the luminosity reached by LEP at the Z pole, generating unprecedented sensitivities producing up to 10^{12} Z bosons [25], see also Figure (1.2). As for the detectors at the FCC-ee, the main proposals made by the FCC collaboration includes two detectors so far, CLD and IDEA. The last one, which will be our focus, is a cylindrical prompt detector planned as a cost-effective instrument with a dual-readout calorimeter. A more recent prompt detector proposal is ALLEGRO (A Lepton collider Experiment with Granular Read-Out) [26], which up until now proposes relevant calorimeter intrinsic energy resolution.

Proposals for improving the search for LLPs include detectors that collect data far from the interaction point (IP), known as far detectors. It is necessary to clarify that, as for now, FCC-ee is not confirmed to host a far detector far from one of it is four interaction points (IPs), but there are initiatives like HECATE (Hermetic CAvern TrackEr) [27] or LAYCAST (Layered CAvern Surface Detector) [28], which are far detectors proposed for future electron-positron colliders like CEPC (Circular Electron-Positron Collider) [29] or FCC-ee, and are proposed to be installed on the cavern hosting the main detector. HECATE is modeled as an hermetic detector that covers the complete solid angle, whereas LAYCAST would be installed only on the walls and ceiling of the cavern, allowing LLPs to escape through the cavern floor. However, LAYCAST represents a more practical and realistic project than HECATE, as building a tracker on the floor is less cost-effective due to the heavy machinery expected to be hosted in the cavern.

This work intends to cover for both of the problems previously mentioned: the possible undetected long-lived particles (LLPs), with the study of HNLs on a region where they behave as LLPs, and the lack of new discoveries at existing collider experiments, studying the possibility of HNLs to be found at the FCC-ee. Our study is motivated by the high luminosity EW scale searches at the FCC-ee, since long lived HNLs within the GeV mass scale can produce a measurable displaced vertex, for small enough heavy-light neutrino mixing. Particularly, we will study the production of two displaced HNLs and their subsequent decays into a muon and two jets at the FCC-ee, operating at the center of mass energy where it will achieve the highest integrated luminosity, the Z pole. We will focus on the $M_N \lesssim M_{Z'}$ parameter space for masses in the 1-100GeV range, exploring benchmarks on the $M_N - |V_{\mu N}|^2$ plane that are still allowed by experimental studies. A summary of these searches can be found in [30] for HNLs in the minimal type I Seesaw, and we note that our work is a bridge between experimental measurements, which are scarce, and purely theoretical predictions for the B-L model, since our final aim is to characterize a signal by simulating an accurate passage of the HNLs through am FCC-ee type detector.

A sensitivity analysis will be conducted for the IDEA+LAYCAST configuration, where HNLs can decay at distances ranging from centimeters, within the IDEA detector, to meters, within the LAYCAST detector, either within or beyond the 5 m radius of IDEA.

Phenomenological analysis of the long lived features of HNLs have been developed mainly for the LHC in the last decade, with increasing interest for electron positron colliders and far detectors in recent years. Generally speaking, the HNL mass can go up to the Grand Unified Theory (GUT) scale, but the displaced searches have been proposed for one of the HNL masses from the GeV scale up to the TeV scale [31][20] in the $U(1)_X$ extension. In the $M_N \sim 100$ GeV scale, LHCb or far detectors proposals like CODEX b or FASER 2 could be sensitive to HNLs predicted in the B-L model for $M_{Z'} < 100$ GeV and a squared mixing as low as 10^{-10} [32]. A TeV scale analysis for electron positron colliders have constrained the $M_N - M_{Z'}$ plane for different decay modes of the HNL on Ref. [33].

In the full $M_{Z'} - g'$ parameter space (without using any effective Lagrangian, as in our work), constraints can be obtained using CONTUR (Constraints on New Theories using Rivet) with LHC data. This gives exclusions of $g' < 10^{-3}$ for $M_{Z'}$ at the order of 1 GeV [34][35]. The LHC has conducted LLP searches that until now have only been able to constrain the minimal HNL model. These HNL searches yield $|V_{lN}|^2 \lesssim 10^{-3}$ for $M_N \lesssim M_{Z'}$ [18]. Experimental constraints like this one leave plenty of parameter space that can be explored by future particle colliders like FCC-ee. Particularly for low values of the mixing squared (under 10^{-13}) and $M_N \lesssim 200$ GeV, the HNLs can decay with lengths of the order of meters [19][36]. If one assumes heavy Z' boson mass (TeV scale), CMS has searched for high mass resonances and constrained $M_{Z'}$ to be bigger than 4.5 TeV [37]. On ref [38] It's shown that displaced vertex signatures can be found for long-lived HNLs on left-right-symmetric models for FCC-ee, CEPC, ILC and CLIC. Another long lived analysis at the FCC-ee was done on [39] for the minimal HNL model.

This thesis is organized as follows: the second chapter is a review of the phenomenology of the B-L model, including neutrino and gauge boson masses. Chapter three is about the simulations for generating and decaying the HNL conducted using MadGraph (`MG5_aMC_v3_5_4`) [40], a Monte Carlo event simulator, and `Pythia 8312` [41], the event hadronizer. Pythia also provides the kinematic statistics of the events. Chapter four is about the complete sensitivity analysis based on the simulated events, starting with the calculation of the probability of decay of an HNL for the geometry of a near and a far detector, IDEA and LAYCAST respectively, followed by the calculation of the number of expected events and the obtained exclusion limit is at 95%CL. A the end of Chapter 4, a brief review, along with preliminary results, is presented concerning the application of the fast simulation software `Delphes 3.5.0` for modeling the IDEA detector with improved accuracy. A final discussion of the results and perspectives for future work can be found in the conclusion.

Chapter 2

Phenomenology of the B-L model

This model of physics beyond the Standard Model consists of the symmetry group $SU(3)_c \times SU(2)_L \times U(1)_Y \times U(1)_{B-L}$, where the SM has been extended to include a new $U(1)_{B-L}$ gauge symmetry [19]. With this, there's a new gauge field B'_μ in the covariant derivative as

$$D_\mu = \partial_\mu + ig_s \mathcal{T}_\alpha G^\alpha_\mu + igT_a W^a_\mu + g_1 Y B_\mu + i\left(\tilde{g}Y + g' Y_{B-L}\right) B'_\mu, \tag{2.1}$$

Where Y_{B-L} and g' are the gauge quantum number and gauge coupling corresponding to the new symmetry and the constant $\tilde{g}$ couples the electromagnetic and B-L gauge sectors. As previously mentioned, the free parameters in a renormalizable model vary with the energy scale. Consequently, certain interactions may decouple from the model at specific energy thresholds, meaning their corresponding couplings can be set to exactly zero or become negligible, removing their contributions to the theory at those scales. This work focuses specifically on the model with $\tilde{g}$ set to zero at the EW scale on the renormalization group evolution. This is the minimal B-L model, where there is no mixing at tree level with the $U(1)_Y$ gauge boson Z. Later we'll see how a new physical gauge boson Z' is constructed with the fields B_μ, B'_μ and W^3_μ, and how it acquires mass through $B-L$ symmetry breaking.

For the B'_μ field there's a new kinetic term,

$$\mathcal{L} \supset F'^{\mu\nu} F'_{\mu\nu}, \tag{2.2}$$

where

$$F'^{\mu\nu} = \partial^\mu B'^\nu - \partial^\nu B'^\mu, \tag{2.3}$$

and the model also includes three heavy neutral leptons in the fermion lagrangian,

$$\begin{aligned}\mathcal{L}_f = \sum_{k=1}^{3} \big(& i\overline{q_{kL}}\gamma_\mu D^\mu q_{kL} + i\overline{u_{kR}}\gamma_\mu D^\mu u_{kR} + i\overline{d_{kR}}\gamma_\mu D^\mu d_{kR} + \\ & + i\overline{l_{kL}}\gamma_\mu D^\mu l_{kL} + i\overline{e_{kR}}\gamma_\mu D^\mu e_{kR} + i\overline{N_{kR}}\gamma_\mu D^\mu N_{kR}\big)\end{aligned} \tag{2.4}$$

where the HNLs, N_{kR}, have the generation index k and are SM singlets. In the scalar sector we have a new Higgs-like singlet scalar particle χ, and the new terms in the scalar potential are

$$V \supset \mu^2|\chi|^2 + \lambda_2^2|\chi|^4 + \lambda_3 H^\dagger H|\chi|^2, \tag{2.5}$$

where H is the SM Higgs doublet. Therefore, the scalar lagrangian is

$$\mathcal{L}_{scalar} = (D^\mu H)^\dagger D_\mu H + (D^\mu \chi)^\dagger D_\mu \chi - V(H, \chi) \tag{2.6}$$

The new particle content and their respective quantum numbers for each symmetry group can be seen on Table (2.1). For a B-L field content table analogous to the one shown in (1.1), see Appendix (A.2).

particle	type	$SU(3)_c$	$SU(2)_L$	$U(1)_Y$	B-L
N_R	fermion	1	1	0	-1
χ	scalar	1	1	0	2
Z'	vector boson	1	0	0	0

Table 2.1: New particle content of the model and their respective quantum numbers.

2.1 Neutrino masses and mixing

In terms of the $SU(2)$ adjoint of the Higgs doublet, $\tilde{H} = i\sigma^2 H^*$, the Dirac adjoint of the SM lepton double,t $\bar{l}_j^T = \begin{pmatrix} \overline{N}_{Lj} & \bar{\ell}_{Lj} \end{pmatrix}$, for $\ell = e$, μ, τ and the charge conjugate of the right handed HNL, $\overline{N}_L^c$, the new Yukawa terms of the model are,

$$\mathcal{L}_Y \supset -y_{jk}^D \bar{l}_{jL} N_{kR} \tilde{H} - y_{jk}^M \overline{N}_{jR}^c N_{kR} \chi \tag{2.7}$$

Following the Higgs mechanism, the Higgs doublets can be parametrized in the Feynmann gauge as:

$$H = \frac{1}{\sqrt{2}} \begin{pmatrix} -i(w^1 - iw^2) \\ v + (h + iz) \end{pmatrix} \text{ and } \chi = \frac{1}{\sqrt{2}} \begin{pmatrix} x + (h' + iz') \end{pmatrix} \tag{2.8}$$

where $w^\pm = w^1 \mp iw^2$, z and z' are the goldstone bosons for the W^+, W^-, Z and Z' respectively. Each scalar boson gets a vacuum expectation value (VEV), v and x, which are real and positive,

$$\langle H \rangle = \frac{1}{\sqrt{2}} \begin{pmatrix} 0 \\ v \end{pmatrix} \text{ and } \langle \chi \rangle = \frac{x}{\sqrt{2}} \tag{2.9}$$

which breaks the $U(1)_Y \times SU(2)_L$ and $U(1)_{B-L}$ symmetries. Consequently, he Yukawa terms for the neutrinos give, following the Seesaw type I mechanism [12],

$$\begin{aligned}\mathcal{L}_Y \supset & -\frac{1}{\sqrt{2}} y^D_{jk}\overline{N}_{jL}N_{kR}v - y^M_{jk}\overline{N}^c_j N_{kR}\frac{x}{\sqrt{2}} + h.c.\\ &= -\frac{m_D}{2}(\overline{N}^c_R N^c_L + \overline{N}_L N_R) - \frac{M}{2}\overline{N}^c_R N_R + h.c.\end{aligned}$$

where we note there's a Dirac mass term for the SM neutrinos and a Majorana mass term for the HNL. The respective mass matrices were defined as

$$m_D = \frac{y^D}{\sqrt{2}}v \quad \text{and} \quad M = \sqrt{2}y^M x, \tag{2.10}$$

and the neutrino generation indices, i, j and k, were omitted, knowing that y^D and y^M are 3×3 matrices. Therefore, in the basis $\begin{pmatrix} N^c_L \\ N_R \end{pmatrix}$ the heavy and light neutrinos mass term can be written as

$$\mathcal{L}_{mass} = \frac{-1}{2}\begin{pmatrix} \overline{N}_L & \overline{N^c}_R \end{pmatrix}\begin{pmatrix} 0 & m_D \\ m_D & M \end{pmatrix}\begin{pmatrix} N^c_L \\ N_R \end{pmatrix} \tag{2.11}$$

The mass matrix can be diagonalized by a rotation by α_ν, such that

$$\tan 2\alpha_\nu = 2m_D M^{-1}, \tag{2.12}$$

and without mixing between generations, the fields N_R and N_L can be written as a linear combination of the mass eigenstates,

$$\begin{pmatrix} N_L \\ N_R \end{pmatrix} = \begin{pmatrix} \cos\alpha_\nu & -\sin\alpha_\nu \\ \sin\alpha_\nu & \cos\alpha_\nu \end{pmatrix}\begin{pmatrix} \nu_1 \\ \nu_2 \end{pmatrix} \tag{2.13}$$

After diagonalizing equation (2.11), in the so-called Seesaw limit ($M \gg m_D$), one gets

$$m_1 \approx -m_D M^{-1} m_D^T \quad \text{and} \quad m_2 \approx M. \tag{2.14}$$

for the SM neutrino and HNL masses respectively. Therefore the heavy and light neutrino mixing is defined by the matrix

$$V_{lN} \approx m_D M^{-1} = \frac{\tan 2\alpha_\nu}{2} \tag{2.15}$$

where $l = e, \mu$ or τ, and in term of the physical masses is

$$\tan 2\alpha_\nu \approx \sqrt{\frac{m_1}{m_2}} \tag{2.16}$$

Thus the neutrino mass scale and the mixing are coupled by the equation,

$$|V_{lN}|^2 \approx \frac{m_1}{m_2}. \tag{2.17}$$

We note that the HNL mass, m_2 in equation (2.17), will be referred to as M_N in the remaining chapters of this work. For values of $m_1 = 1eV$ for the SM neutrino mass and $m_2 = 100\text{GeV}$ for the HNL, $\tan \alpha_\nu \sim 10^{-5}$ and since α_ν is small, the mixing is of the same order. Since the HNL are only allowed to decay via this mixing matrix, this value results in long lived HNLs due to the suppressed decay width Γ, to be elaborated on shortly. However, to simplify the task of proposing a displaced HNL search and maximize the possible patterns, we decouple the mixing and HNL mass, scanning them independently and disregarding neutrino oscillation constraints. Our scan will take values for the HNL mass in the scale of the GeV and $|V_{lN}|^2 < 10^{-4}$ for the mixing, since our interest is in long lived HNLs. In our phenomenological analysis, the mixing matrix will feature a single non-zero component, effectively coupling only one SM neutrino flavor with one HNL flavor, $l = \mu$.

For simplicity, the Heavy Neutral Lepton (HNL) will be referred to as N throughout the remainder of this thesis.

2.2 Gauge boson masses

Finally, we'll see how the scalar kinetic terms

$$(D^{\mu}H)^{\dagger}D_{\mu}H + (D^{\mu}\chi)^{\dagger}D_{\mu}\chi \tag{2.18}$$

give masses to the Z', Z, $W^{\pm}$ bosons and particularly how the definite mass physical fields A^{μ}, Z^{μ} and Z'^{μ} are conformed by a mixing of the B^{μ}, B'^{μ} and W^{+} fields after EW and B-L symmetry breaking. Using the covariant derivative on (2.1) and omitting the $SU(3)$ terms, if we use the unitary gauge, [42]

$$H = \frac{1}{\sqrt{2}}\begin{pmatrix} 0 \\ v+h \end{pmatrix} \quad \text{and} \quad \chi = \frac{1}{\sqrt{2}}(x+h') \tag{2.19}$$

then we have

$$(D^{\mu}H) = \frac{1}{\sqrt{2}}\begin{pmatrix} \partial^{\mu} + \frac{i}{2}(gW^{(3)\mu} + g_1B^{\mu} + \tilde{g}B'^{\mu}) & \frac{i}{2}g[W^1 - iW^2] \\ \frac{i}{2}g[W^1 + iW^2] & \partial^{\mu} - \frac{i}{2}(gW^{(3)\mu} - g_1B^{\mu} - \tilde{g}B'^{\mu}) \end{pmatrix}\begin{pmatrix} 0 \\ h+v \end{pmatrix}$$

and

$$(D^{\mu}\chi) = \frac{1}{\sqrt{2}}(\partial^{\mu} + 2ig'B'^{\mu})(h'+x), \tag{2.20}$$

where we used $Y_{B-L} = 2$ and $Y = 0$ for the scalar field χ, $Y_{B-L} = 0$ and $Y = 1/2$ for the Higgs doublet H. Therefore,

$$\begin{aligned}
&(D^\mu H)^\dagger D_\mu H + (D^\mu \chi)^\dagger D_\mu \chi = \\
&\frac{1}{8}\Big[[gW^{(3)\mu} - g_1 B^\mu - g' B'^\mu](v+h)^2[-gW^{(3)}_\mu - g_1 B_\mu - g' B'_\mu] - \\
&g^2[W^{(1)\mu} - iW^{(2)\mu}][W^{(1)}_\mu + iW^{(2)}_\mu](v+h)^2\Big] + \frac{1}{2}\partial^\mu h \partial_\mu h \\
&\frac{1}{2}\partial^\mu h' \partial_\mu h' + \frac{1}{2}(x+h')^2(2g' B'^\mu)^2
\end{aligned}$$

We notice that the $W^\pm$ masses appear just like in the SM, and the terms involving B^μ, $W^{(3)\mu}$ and B'^μ can be rewritten as

$$\begin{pmatrix} B^\mu & W^{(3)\mu} & B'^\mu \end{pmatrix} M_1 \begin{pmatrix} B^\mu \\ W^{(3)\mu} \\ B'^\mu \end{pmatrix} \tag{2.21}$$

where M_1 is the non diagonalized matrix. After diagonalizing, one finds that the mass eigen states A_μ, Z_μ and Z'_μ are written in terms of the gauge fields W^3_μ, B_μ and B'_μ, in analogy with the SM:

$$\begin{pmatrix} B^\mu \\ W_3{}^\mu \\ B'^\mu \end{pmatrix} = \begin{pmatrix} \cos\vartheta_w & -\sin\vartheta_w\cos\vartheta' & \sin\vartheta_w\sin\vartheta' \\ \sin\vartheta_w & \cos\vartheta_w\cos\vartheta' & -\cos\vartheta_w\sin\vartheta' \\ 0 & \sin\vartheta' & \cos\vartheta' \end{pmatrix} \begin{pmatrix} A^\mu \\ Z^\mu \\ Z'^\mu \end{pmatrix} \tag{2.22}$$

where ϑ', the $U(1)_Y$ and $U(1)_{B-L}$ mixing angle, is defined through the expression

$$\tan 2\vartheta' = \frac{2\widetilde{g}\sqrt{g^2+g_1^2}}{\widetilde{g}^2 + 16\left(\frac{x}{v}\right)^2 g'^2 - g^2 - g_1^2}. \tag{2.23}$$

After diagonalizing the mass matrix one gets $M_A = 0$ for the photon for any $\tilde{g}$ value. In the minimal model, where $\tilde{g} = 0$, one can calculate that $\vartheta' = 0$, and thus there is no mixing between the Z and Z' bosons. Under this condition, the expression for the Z boson mass is identical to the SM, thus the EW masses are independent of the B-L parameters and vice versa, the B-L gauge boson does not depend on the weak parameters:

$$M_Z = \frac{v}{2}\sqrt{g^2 + g_1^2} \text{ and } M_{Z'} = 2g'x. \tag{2.24}$$

The free parameters to be scanned in our simulations are given in Table (2.2).

parameter	description
g'	B-L gauge coupling
$M_{Z'}$	Z' boson mass
M_N	HNL mass
$\lvert V_{\mu N}\rvert^2$	heavy light neutrino mixing

Table 2.2: Relevant parameters of the model used to simulate the Monte Carlo events.

The Z' boson partial decay width to two HNL's is calculated numerically by MadGraph and is given by

$$\Gamma(Z' \to NN) = \frac{1}{6}\frac{g'^2}{2\pi} m_{Z'}\left(1 - 4\frac{m_N^2}{m_{Z'}^2}\right)^{3/2}. \tag{2.25}$$

And the corresponding cross-section for an electron-positron pair producing an on-shell Z' which decays into two HNL's is therefore proportional to g'^2. Detailed studies on cross sections can be found in ref. [33]. The Feynmann rules involving HNLs in our process can be seen in Appendix. (A.1)

Chapter 3

Z' and HNL Production and Decay

3.1 HNL production

We numerically compute production cross-sections and decay rates for an HNL implementing the B-L model in a Monte Carlo Software widely used in High Energy Physics simulations, called Madgraph (`MG5_aMC_v3_5_4`) [40]. MadGraph is a computational tool that generates events for particle collisions based on theoretical models in quantum field theory. It takes as input a specified model with its corresponding Feynman rules to compute matrix elements and cross-sections for the given process, employing numerical methods when necessary to handle complex calculations. This software performs Monte Carlo cal-

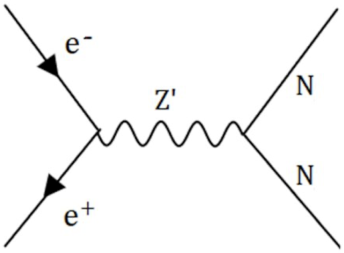

Figure 3.1: Feynmann diagram for the process simulated in MadGraph 3.5.4, where Z' is a new gauge boson and N is a heavy neutral lepton.

culations to evaluate the integrals of matrix elements over a multidimensional parameter region. The specified model must comprehensively define all particle properties, including names, quantum numbers, mass, spin, and decay modes, along with couplings, propagators, and interaction vertices. This ensures an accurate representation of the particle interactions and dynamics during the event generation. Event simulators like MadGraph take models defined with Universal FeynRules Output (UFO) files [43] and, particularly in this work, the B-L model was implemented with the UFO file used in [20].

After the model is implemented via the UFO file, the specifications of each simulation need to be set manually, indicating the process to simulate and the values for the free parameters of the model, enlisted in Table (2.2) for the minimal B-L model. Along with this, the specifications of each simulation have to be set each time as well: the number of Monte Carlo events, the energy of the particle beams, and the chosen decay strategy for the resulting particles to reflect the intended physical scenario. In this work, the beam energies were configured to be half of the center-of-mass (COM) energy of 91 GeV. It is noteworthy that using only MadGraph provides important outputs such as cross-sections, decay widths, and branching ratios for the particles involved in the specified process.

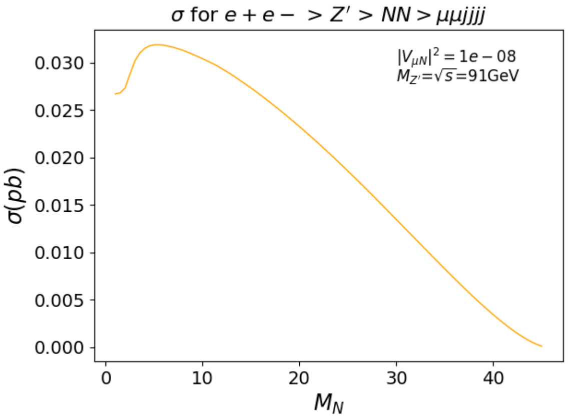

Figure 3.2: Cross section at $\sqrt{s} = 91$ GeV for the process $e^+e^- \to Z' \to NN \to \mu\mu jjjj$ as a function of the HNL mass for a fixed value of $M_{Z'}$ and $|V_{lN}|^2$.

The process $e^+e^- \to Z' \to NN \to \mu jjjj$ (Fig. (3.1)) was simulated with Madgraph event generator, scanning the parameters g', M_N, $M_{Z'}$ and $|V_{lN}|^2$. Two values of the coupling g' were chosen, 10^{-3} and 10^{-4}, and mass ranges were explored within the region $M_N \lesssim M_{Z'}$. First, we scanned three values for the mass of the Z' boson, $M_{Z'}$: 91 GeV, 250 GeV and 1 TeV, for a center of mass energy $\sqrt{s}$ reaching up to the TeV scale with a fixed HNL mass of $M_N = 5$ GeV. With these values, we plotted the corresponding resonances on $M_{Z'} = \sqrt{s}$. Additionally, we scanned M_N from 1 GeV to 45 GeV, intending to plot the HNL's Branching Ratio (BR) and generating sensitivity curves for the peak $M_{Z'} = \sqrt{s} = 91$ GeV. All the scanned parameters are listed in Table (3.1).

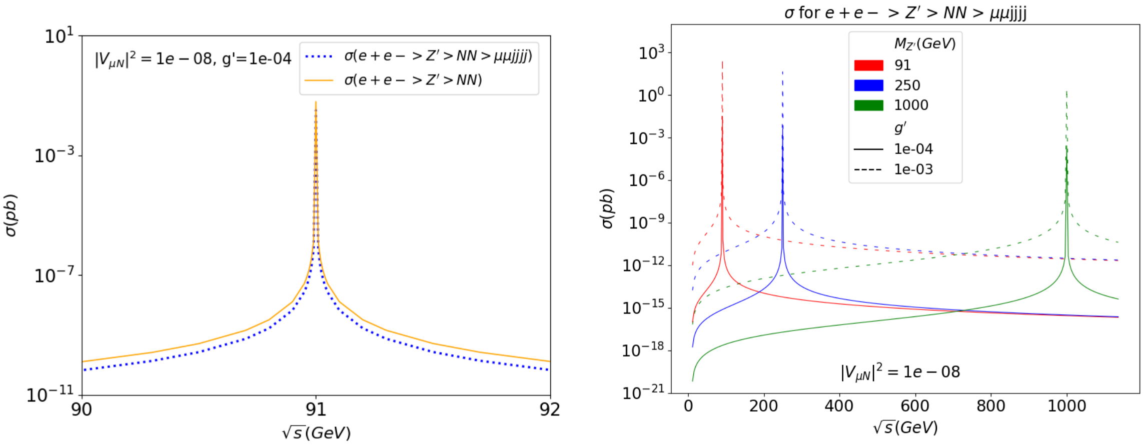

((a)) ((b))

Figure 3.3: Cross-section as a function of the center of mass energy for the process $e^+e^- \to Z' \to NN \to \mu\mu jjjj$. Figure a) shows the Z pole for a decayed and a not decayed HNL. Figure b) shows the same cross-section for Z' masses of 91, 250 and 1000 GeV and a B-L coupling of $g' = 10^{-3}$ and 10^{-4}.

As already stated, the B-L model was simplified in the simulation to contain only one HNL in the kinematic region of interest, and the other two HNL masses were set at 10^4 GeV such that they are decoupled from the FCC-ee reach. As for the heavy-light neutrino mixing, only the $|V_{\mu N}|$ component was set to a non-zero value. Consequently, HNL decays in our case result exclusively in muons, although the final state may also include other leptons via the W boson generated in the $N \to \mu W$ channel. Our chosen channel for the HNL will be the one where the W boson decays into a pair of jets.

A cross-section up to 612pb was obtained for the mentioned process with $g' = 10^{-3}$ and 0.0612 pb with $g' = 10^{-4}$ for $M_{Z'} = \sqrt{s} = 91 GeV$. These values agree with the g'^2 dependence of the cross-section according to the Feynmann rules for the simulated process (see appendix (A.1) and Figure (3.1)). A cross-section plot as a function of the HNL mass for fixed $\sqrt{s} = 91$ GeV is shown on Figure (3.2), also, a cross-section plot for the decayed and not decayed HNL as a function of the HNL mass can be seen in Figure (3.3), along with the cross-section up to 1 TeV of center of mass energy for two g' values. The factor between the two cross-sections is of around 0.5 according to the BR plot in Figure (A.2) and the Narrow Width Approximation (NWA), which states that $\sigma(e^+e^- \to Z' \to NN \to \mu\mu jjjj) = \sigma(e^+e^- \to Z' \to NN) \times BR^2(N \to \mu jj)$, although we note that, in our analysis, MadSpin [44] (referred to in detail later) provides the full non-approximated result.

Parameter	Scan
$M_{Z'}$	91, 250, 1000
M_N	1 - 45
g'	1e-03, 1e-04
$\sqrt{s}$	300 val for 1-110
$\lvert V_{lN}\rvert^2$	1e-20 - 1e-08

Table 3.1: B-L parameter space simulated in MadGraph (`MG5_aMC_v3_5_4`). All energy and mass values are given in GeV.

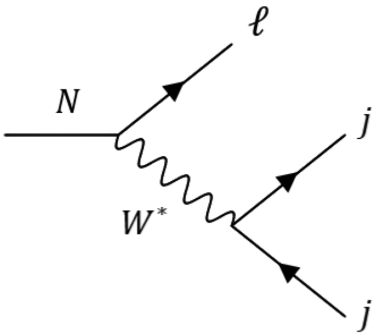

Figure 3.4: Chosen decay channel for the HNL through an off-shell W boson, where $\ell = \mu$ in the simulated events.

3.2 HNL decay

The HNL decay was specified in the MadGraph script to be performed using MadSpin[44], which is integrated into MadGraph and handles particle decays while accounting for spin correlations in the process (as opposed to only using MadGraph, which does not). This is particularly important when there is an intermediate weak boson, since generally speaking the resulting quark distributions can be sensitive to the initial spin states, because weak interactions depend on the chirality of the particles involved in the production of said weak boson.

The chosen decay channel for the HNL is $N \to \mu jj$, as shown in Fig. (3.4). A BR plot for the HNL is shown in Figs. (A.2) and (A.3), where the μjj channel can be seen. It is important to note that for each of these BR plots, the simulation included only one accessible HNL, which decayed according to its corresponding lepton flavor dictated by a diagonal mixing matrix with only one non-zero matrix element. Therefore, the BR plots in Figures (A.2) and (A.3) are independent between each other (which means that they sum 1 separately), and each represents a simplified model where N_1 decays into electrons (through $|V_{e1}|$) or N_2 decays into muons (through $|V_{\mu 2}|$). Since these two independent situations produce the same BR plot, only one was shown. The case where we have a model with one HNL, N_3 which decays only into taus (through $|V_{\tau 3}|$) is shown in Figure (A.3). As previously mentioned, we simulate a muon-type HNL, and the others are shown for comparison purposes.

In the search for long lived particles its of special importance the proper decay distance of the particle, $c\tau$, where τ is the proper time and c is the velocity of light in vacuum. Therefore, for HNLs [36],

$$c\tau = \frac{c\hbar}{\Gamma} \sim \frac{c\hbar}{m_N^5 G_F^2 |V_{\ell N}|^2} \tag{3.1}$$

where G_F is the Fermi constant and Γ is the total decay width of the HNL. The explicit expression for the HNL decay width have been omitted for simplicity and is calculated numerically by the mentioned software. In Figures (3.7(a)) and (3.7(b)), a $c\tau$ plot is shown for various squared heavy-light mixings, with a colored band in the background indicating the inner and outer dimensions of the IDEA detector sections: vertex finder, drift chamber, and calorimeter + muon system (see Table (4.1), along with the distance to the LAYCAST half-length [5 m, 20 m]. $c\tau$ was calculated using equation (3.1) and from the plot we can see that in the 1 GeV - 45 GeV range for M_N, IDEA has an acceptance down to $\sim 10^{-12}$ on mixing squared.

The boost factor is defined as

$$\beta\gamma = \sqrt{(E/M_N)^2 - 1}, \tag{3.2}$$

where E and M_N are the energy and mass of the HNL respectively, and the decay length can be expressed as boosting the propper distance $c\tau$,

$$\lambda = \beta\gamma c\tau. \tag{3.3}$$

A plot for these observables is shown in Figures (3.8) and (3.9). For these plots, the decay length was calculated as the difference between the decay and the production coordinates for each particle using the functions `.xDec()` and `.xProd()` of the `Pythia 8` software [41] for each coordinate, and it was cross checked that equation (3.3) holds. For similar plots for the decay length and the boost factor projected to the z axis, see Appendix (A.3).

After `MadSpin` generates the decays, parton showering and hadronization are handled by `Pythia 8312` [41], a software that extends MadGraph processing the MadGraph+MadSpin output in the form of a Les Houches Event file (`.lhe`)[45]. As mentioned, Pythia simulates soft QCD processes and particle decays, generating Monte Carlo events for the given process. From Pythia, kinematic information such as the four momenta and the angles for all particles involved in the process are obtained, starting from the initial electron positron pair to all the resulting daughter particles after parton shower is done by the software. In our simulation, two HNLs were found in every event, as expected.

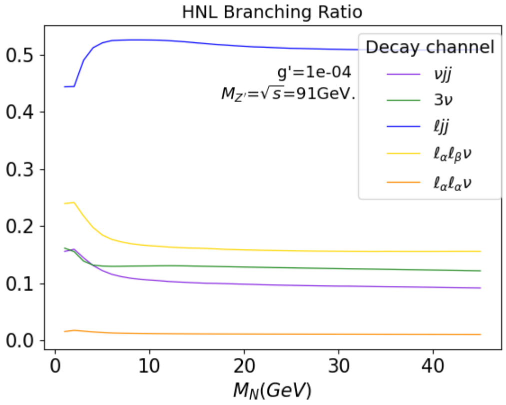

Figure 3.5: Branching Ratios for the simplified choice of one HNL decaying into only one type of lepton ℓ for $\ell = \mu$ or e and $|V_{\mu N}|^2 = 10^{-8}$.

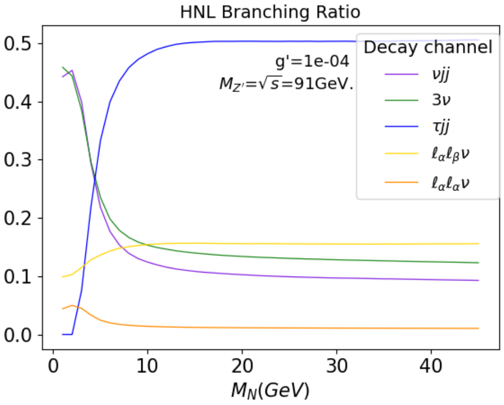

Figure 3.6: Branching Ratios for the simplified choice of one HNL decaying into only one type of lepton τ, for $|V_{\mu N}|^2 = 10^{-8}$.

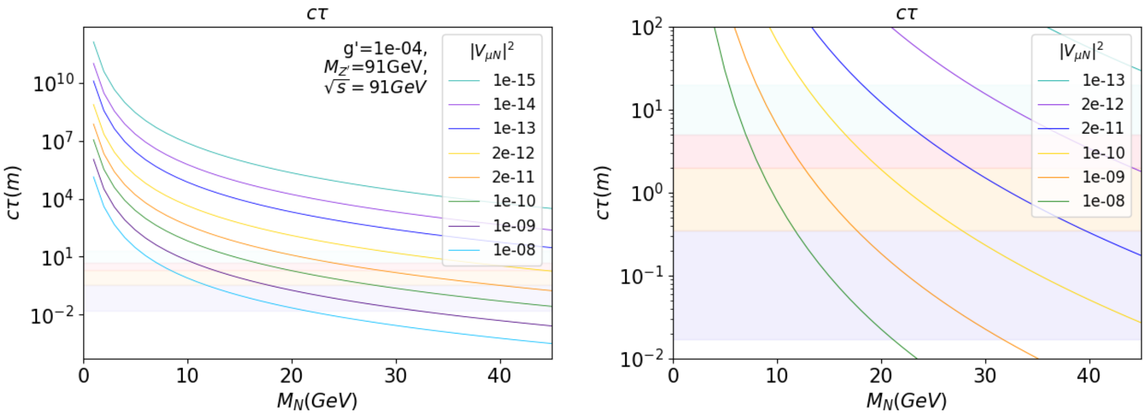

((a)) ((b))

Figure 3.7: a) $c\tau$ vs HNL mass for different values of the heavy-light mixing squared. The colored bands in the background are the inner and outer distances for different sections in the IDEA+LAYCAST configuration, from bottom to top: IDEA's vertex finder (purple region), IDEA's tracker technology (drift chamber, orange), IDEA's calorimeter+muon system (red) and finally, distance to one of LAYCAST's walls (light blue). b) Zoomed in plot.

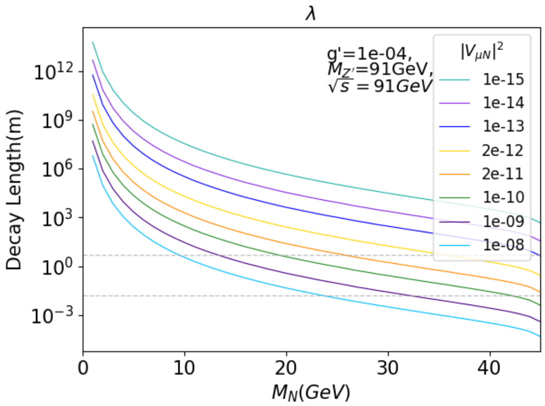

Figure 3.8: Decay length as a function of the HNL mass for different mixings. Dashed lines determine IDEA's inner and outer radius.

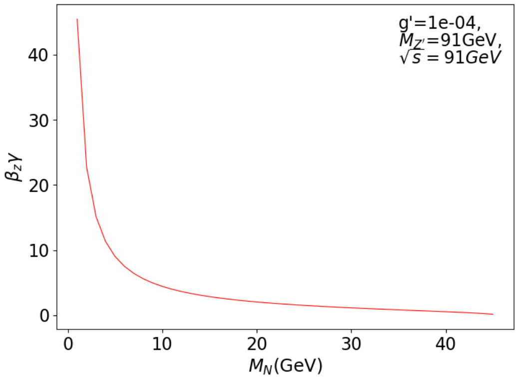

Figure 3.9: Boost factor as a function of the HNL mass.

The kinematic data for their lepton daughters are written in terms of the spherical coordinates and four-momenta $p^\mu = (E, \vec{p})$ of the particles (muons, in this case), such as the transverse momentum $p_T = \sqrt{p_x^2 + p_y^2}$, transverse energy $E_T = p_T sen(\theta)$, rapidity $y = ln((E + p_z)/(E - p_z))/2$ and pseudorapidity $\eta = -ln(tan(\theta/2))$, are shown in Figure (3.10). This variables would be the MC generated theoretical prediction, to be compared with the detector-simulated data after being passed through a software like Delphes [46], which accurately simulates the passage of the particles through the detector components such as trackers, calorimeters and the muon system. A similar plot for the HNLs is shown in Figure (3.11). θ and ϕ of each HNL will be used event-by-event in the calculation of the probability of decay inside the fiducial volume for IDEA and LAYCAST. θ will be used to determine the projection of the distances along the z-axis, and the azimuthal angle, ϕ, will be used to determine the acceptance of LAYCAST, which isn't symmetric with respect to this angle.

We note that for muons and HNLs ϕ is distributed uniformly and the θ distribution peaks around 60° and 120°. The production of low energy muons is most probable, although, as being produced along with an of-shell W boson, the energy values are not kinematically bounded. From the p_T plot for the produced HNLs we note that p_T is very close to $p = 45$ GeV, which is the maximum kinematically allowed energy for the HNL, and since the HNL mass in this plot is 5 GeV, we can conclude that the longitudinal component of the momentum is small compared with the transverse one.

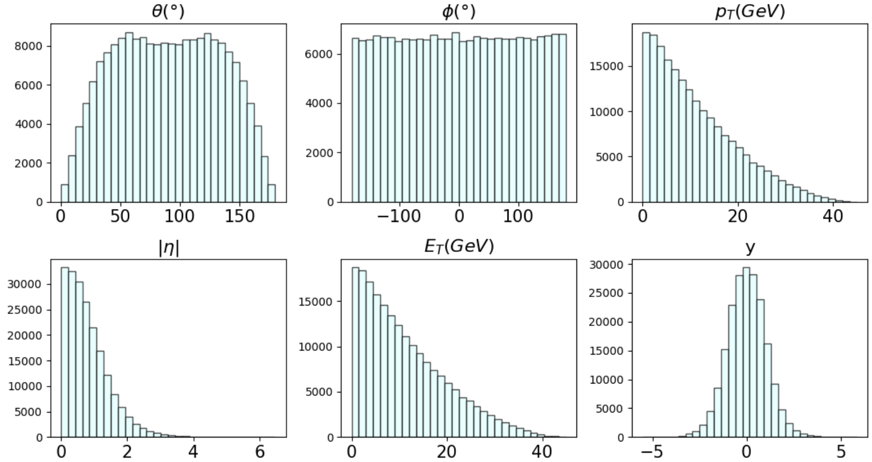

Figure 3.10: Kinematic variables of the final-state muons produced by an HNL with mass of $M_N = 5$GeV and $|V_{lN}|^2 = 10^{-8}$ through the channel $N \to \mu jj$, obtained using Pythia 8.

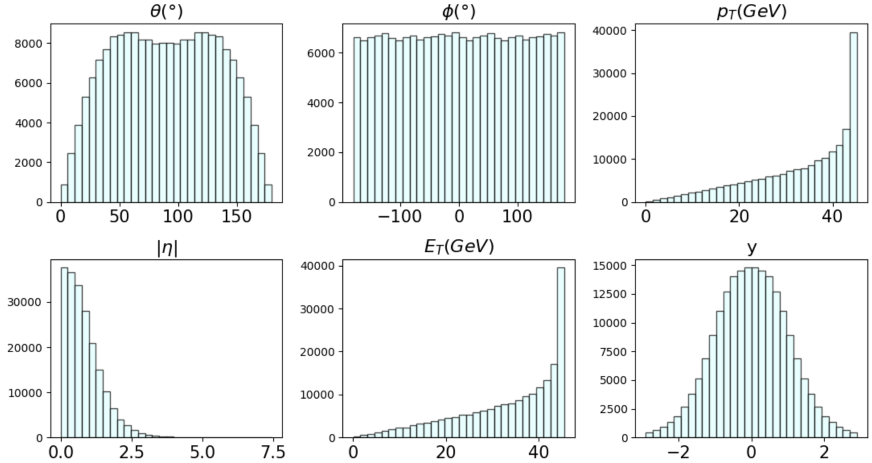

Figure 3.11: Kinematic variables of the HNLs with a mass of $M_N = 5$GeV and $|V_{lN}|^2 = 10^{-8}$, produced in the process $e^+e^- \to Z' \to NN \to \mu\mu jjjj$, which were obtained using Pythia 8.

Chapter 4

Displaced HNL signals at the FCC-ee

Theoretically, the number of events for a given process is given by [47]

$$n = \sigma \times \mathcal{L} \tag{4.1}$$

where $\mathcal{L}$ is the integrated luminosity, a measure of the event rate, and σ is the cross-section of the process. In the case of imperfect detection, the number of expected events is defined as

$$\mathcal{N} = \sigma \times \mathcal{L} \times \epsilon \tag{4.2}$$

where ϵ is a factor that accounts for both the geometrical acceptance and the efficiency of the detector.

In this chapter, we will first present a way of calculating ϵ as an acceptance factor represented by a probability of decay inside of the fiducial volume for a perfect detector, using the software `Pythia 8312`. Next, we will use this factor to calculate the number of expected events for the process $e^+e^- \to Z' \to NN \to \mu\mu jjjj$ and generate sensitivity curves. Finally, preliminary results will be shown for the case of applying the fast simulation software `Delphes 3.5.0` on the calculation of an efficiency factor that takes into account the geometry and performance of the detector.

4.1 A Geometrical Analyses: The Probability of Decay

4.1.1 IDEA detector

The IDEA detector is a 5 meter radius cylinder of 13 meters length planned for the FCC-ee [25]. A diagram showing the geometry of the cylindrical detector's fiducial volume can be seen in Figure (4.1). And the respective detector's parts and sizes are given in Table (4.1).

The vertex finder (VF) is the part of the detector that is responsible for identifying the point of origin of particle tracks. The drift chamber is a tracking detector that measures the trajectory of the charged particles by detecting the ionization produced in gas when charged particles pass through it, allowing momentum reconstruction. The dual readout calorimeter is an electromagnetic and hadronic detector designed to measure the energy energy of particles, with electromagnetic calorimeters detecting electrons and photons through scintillation, while hadronic calorimeters measure the energy of hadrons through Cherenkov radiation. Additionally, the muon system is designed to detection of muons, which can penetrate through the calorimeter and the tracking detectors. This system consists of tracking detectors and calorimeters optimized for high-precision measurements of muons, enabling their identification and precise momentum determination in the final state of particle collisions.

The probability for a particle to decay inside such a detector is given as a function of the polar angle θ_i for the i-th simulated HNL,

$$P(\theta_i) = e^{-L_1(\theta_i)/\lambda_i^z}(1 - e^{-L_2(\theta_i)/\lambda_i^z}), \tag{4.3}$$

where λ_i^z is the decay length of the HNL along the z axis[1], $L_1(\theta_i)$ is the distance from the interaction point (IP) to the point where the particle enters the detector section and $L_2(\theta_i)$ is the distance from $L_1(\theta_i)$ to the point where the particle exits the detector. Both distances are calculated projected to the beam axis (z), as can be seen in Figure (4.1). This geometrical parameters are given by the equations

$$L_1(\theta_i) = \frac{R_I}{tan(\theta_i)} \tag{4.4}$$

$$L_2(\theta_i) = min\left(\frac{R_O}{tan(\theta_i)}, \frac{L_D}{2}\right) - L_1(\theta_i) \tag{4.5}$$

where the minimum function makes sure that the horizontal distance traveled by the particle through the detector is never longer than the detector length.

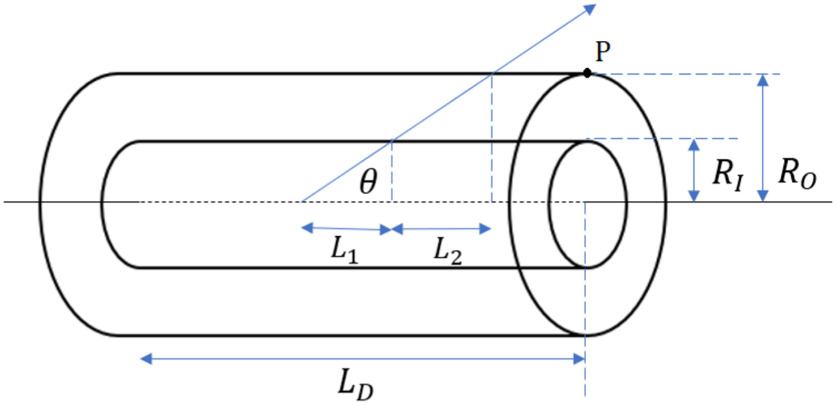

Figure 4.1: Schematic representation of the section o a cylindrical detector like IDEA. The distances projected to the beam axis are used for the calculation of the probability of an HNL decaying in the fiducial volume of the detector (L_1 y L_2), along with the detector length (L_D), inner (R_I) and outer (R_O) radius.

---

[1] λ_z is calculated in `Pythia 8312` as `event[i].zDec() - event[i].zProd()` for the i-th particle in the event.

IDEA section	R_I	R_O	L_D
Vertex Finder	0.017	0.34	1.05
Drift chamber	0.34	2	2
Cal + muon system	2.5	5	13

Table 4.1: Dimensions in meters for the different IDEA detector sections, [25].

To calculate the mean probability of decay of an HNL decaying inside the fiducial volume of a cylindrical detector for each benchmark with N simulated events, the mean is taken over the N simulated events as

$$\langle P(\theta) \rangle = \frac{1}{\mathrm{N}} \sum_{i}^{\mathrm{N}} e^{-L_1(\theta_i)/\lambda_i^z}(1 - e^{-L_2(\theta_i)/\lambda_i^z}). \tag{4.6}$$

The decay length λ_z, and thus the probability, depends on the HNL mass and mixing with SM neutrinos as seen in Figures (4.2) and (4.3). For the first plot, the HNL mass was scanned from 1 GeV to 45 GeV with a fixed mixing of $|V_{\mu N}|^2 = 10^{-9}$. The detector dimensions introduced in the probability equation correspond to the Vertex Finder (VF) system of IDEA, and all of them are listed in Table (4.1). It can be observed that the most probable decay length in this case is 0.24 mm, inside the VF, as expected for the probability distribution which decays exponentially.

For Figure (4.3), the squared mixing was scanned from 10^{-8} to 10^{-20} for fixed HNL masses of 5 GeV, 20 GeV, and 40 GeV. It can be seen that the most probable decay length is also independent of the HNL mass, since fixing different values of the HNL mass results in the same probability curve. In this case, the probability peaks at 0.13m, which is approximately the same as the one from Figure (4.2) if we compare them with all their decimals. It was also noted that this peak does not change as the mixing changes. The described behavior is expected because the most probable decay length depends only on the geometry of the detector, that is introduced through the probability calculation. This argument can result more clear by considering that, for a fixed detector geometry and no projection in the z axis (for simplicity of the argument), the probability function can be maximized for a certain λ, and such maximum will only change by changing the lengths of the detector parameters (once the HNL kinematics is fixed).

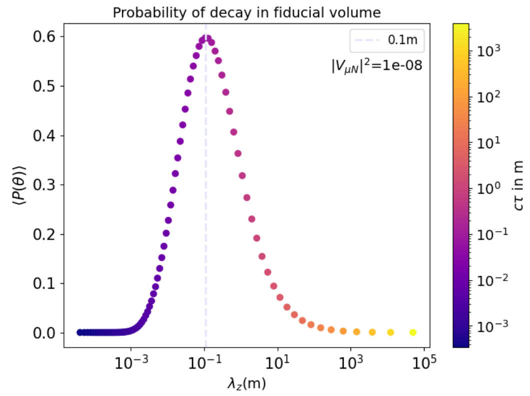

Figure 4.2: Probability of an HNL decaying in the fiducial volume of the Vertex finder in the IDEA detector at the FCC-ee, for fixed value of the mixing and varying the projected decay length λ_z with the value of the HNL mass.

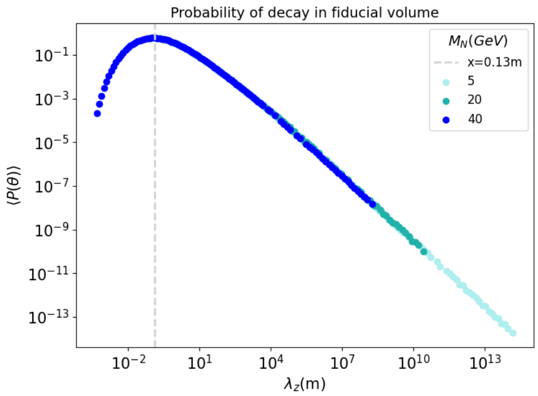

Figure 4.3: Same probability as in Fig. (4.2) but for a fixed value of the HNL mass, varying the projected decay length λ_z by varying the heavy-light squared mixing between 10^{-20} and 10^{-8}.

4.1.2 LAYCAST: A Far Detector Porposal

A key necessity in the search for long lived particles is to build detectors that have sensitivity to particles which are produced far away from the interaction point, as a result of the decay of a long lived particle (could be from meters to tenths of meters), known as far detectors. These detectors are usually proposed as a secondary detector working alongside a "prompt" one (where the collision happens), which is most sensitive to particles that decay promptly, below the millimeter scale.

We will consider a far detector modeled as a square cuboid laying outside a main detector like IDEA. The probability of an HNL decaying inside such a detector is calculated in a similar way as the one just shown for a cylinder, specifically in the case where the "square" far detector is centered on the IP. In the case of LAYCAST (LAYered CAvern Surface Tracker)[28], which is a far detector proposed for the IDEA detector at the FCC-ee (see Figure (4.4)), it consists of a tracker system installed all around the walls and ceiling of the cavern where the IDEA detector will be installed, which it is simplified into a box. It is characterized by the fact that it is not symmetrical around the vertical axis with respect to the IP, and therefore the azimutal ϕ angle is partially covered. For such a detector, the probability was calculated following the procedure in ref. [48], using equation (4.6), with $L_1(\theta)$ and $L_2(\theta)$ given by

$$L_1(\theta) = min\left(\frac{L}{2}, \frac{R_O}{tan(\theta_i)}\right), \tag{4.7}$$

$$L_2(\theta) = min\left(\frac{L}{2}, \frac{D}{tan(\theta_i)}\right) - L_1(\theta), \tag{4.8}$$

and R_O being the outer radius of the prompt detector, which would be 5 m for IDEA. Therefore, two reference points are taken: the exit point through the cylindrical main detector and the arrival point at the squared far detector. In the case of IDEA, our points were the entry and exit of the cylindrical section. Its important to mention that, as the name says, LAYCAST is a "cavern-like" tracker box without any material or detection technology in the bulk of the separation between the two detectors.

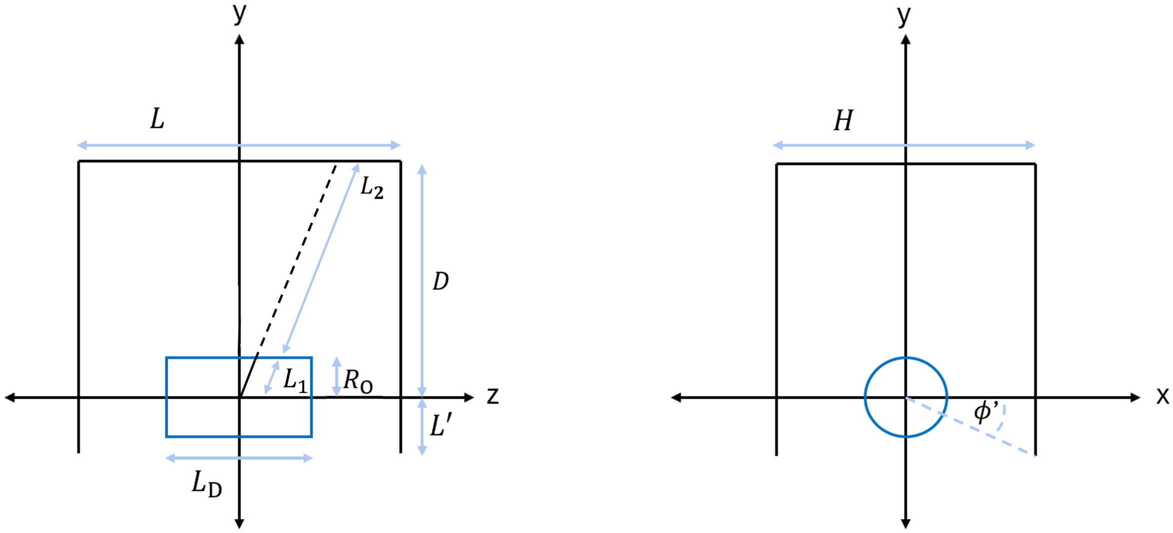

Figure 4.4: IDEA+LAYCAST configuration centered on the IP. L_D and R_O are the length and radius of the cylindrical prompt detector. The particle's path inside the prompt detector is L_1, drawn with a solid line, and inside the LAYCAST fiducial volume L_2, drawn with a dashed line.

The dimensions for LAYCAST can be seen in Table (4.2). The ϕ coverage is $[-26.57°, 307.57°]$, given by the angle $tan(\phi') = 2L'/H$ on Figure (4.4), and $P(\theta)$ is manually imposed to be zero for HNLs that go in the direction of the floor, by dropping those HNLs with azimutal angles outside of this range. An analogous way of accounting for the ϕ coverage would be by multiplying the probability by a fixed factor of $\alpha/2\pi$, where $\alpha = \arctan H/2(D + L')$, as it was done in ref. [48]. The dimensions for LAYCAST can be seen on Table (4.2).

Length	L	H	D	L'
Value	40	20	25	5

Table 4.2: Dimensions in meters of the IDEA+LAYCAST configuration. D is the height of LAYCAST above the IP, and L' is the length of the tracker system below it, taking y as the height coordinate. L is the width in the z direction and H is the width in the x direction.

4.2 Number of Expected Events

In order to estimate the reach of a certain detector over a set of free parameters, its necessary to calculate the number of expected events for a determined process of interest. In our case, we calculated it for the process already shown, with the HNL pair produced from a Z' boson and decaying to μjj at the FCC-ee. With this, one can obtain a sensitivity plot and, for a specific number of expected events $\mathcal{N}$, determine a contour over a determined parameter space that constrains the particular model used, that is, the chosen geometry and the fixed parameters. These sensitivity curves provide an exclusion under non-signal observation in that parameter space, which we identify as a region with experimental sensitivity. Therefore we are able to propose a specific search for detectors to test the minimal B-L model.

The number of expected events for our process is given by

$$\mathcal{N} = 2 \cdot \sigma(e^+e^- \to Z' \to NN \to \mu\mu jjjj) \cdot \mathcal{L} \cdot \langle P(\theta) \rangle \tag{4.9}$$

where $\langle P(\theta) \rangle$ is the probability for the HNL to decay inside of the fiducial volume, averaged over the N events of the Monte Carlo simulation (different from $\mathcal{N}$, the number of expected events, and from N, the HNL). We followed the procedure explained in the last section for calculating the probability of decay inside the FV, $\langle P(\theta) \rangle$, using the projected decay length λ_z as input for IDEA and LAYCAST, as the one shown in Figure (4.2) for a chosen fixed squared mixing of $|V_{\mu N}|^2 = 10^{-8}$. With these results, a number of expected events $\mathcal{N}$ was calculated for each fixed benchmark of our free parameters, M_N, $M_{Z'}$, g', $|V_{\mu N}|^2$, and $\sqrt{s}$. Two of these points can be found in Appendix (A.4), including these parameters and other observables like $c\tau$ and cross-section.

In order to analyze the capability of the IDEA detector to detect long-lived HNLs, an exclusion sensitivity region under the zero background assumption (for which $N = 3$ gives a 95%CL exclusion limit) will be presented in two planes, $M_N - M_{Z'}$ and $M_N - |V_{\mu N}|^2$. These planes will be explored for multiple run-times, scanning 10^4 points for each plot, and $N = 50k$ Monte Carlo (MC) events for each point. In the $M_N - |V_{\mu N}|^2$ plane, for squared mixings around 10^{-14} and below, Pythia fails to process a significant number of MC events, therefore the statistics becomes poor and the probabilities come out irregular. The fluctuations in the probability of decay die quickly when upgrading the simulation to $N = 100k$ MC events, but the computational power required increases at the same rate, particularly because we are generating the decays with MadSpin, so the amount of MC events was increased to $70k$ events only in the indicated mixing range.

In the benchmark $g' = 10^{-3}$, $\sqrt{s} = 91$ GeV, with M_N within the mass range 1 GeV - 45 GeV and $M_{Z'}$ in the range 10^{-1} GeV-10^3 GeV, the IDEA detector only shows sensitivity around the $M_{Z'} = \sqrt{s}$ enhancement in the $M_N - M_{Z'}$ plane, as seen in Figures (4.6) and (4.8), as dictated by the peak of the cross-section (Figure (3.3)). In Figure (4.8) we see that the constraint over the parameters in this plane cannot be done for $g' = 10^{-4}$, where the sensitivity plot shows a narrow pic on the benchmarks with $M_{Z'} = \sqrt{s}$ due to the loss on cross-section for smaller g', after 4 years of runtime (which corresponds to an integrated luminosity of $150 \cdot 10^6\ pb^{-1}$ according to Figure (1.2)). This plot is mostly symmetric around the $\sqrt{s}$ enhancement and is wider for lower values of the HNL mass. The slight asymmetry can be observed along the M_Z' axis, where the reach to the left of the constraint is half a GeV larger than the right reach towards higher mass values. This comes from the values of the cross-section as a function of $M_{Z'}$, which show a very slightly higher value for $M_{Z'}$ approaching the 91 GeV enhancement from the left.

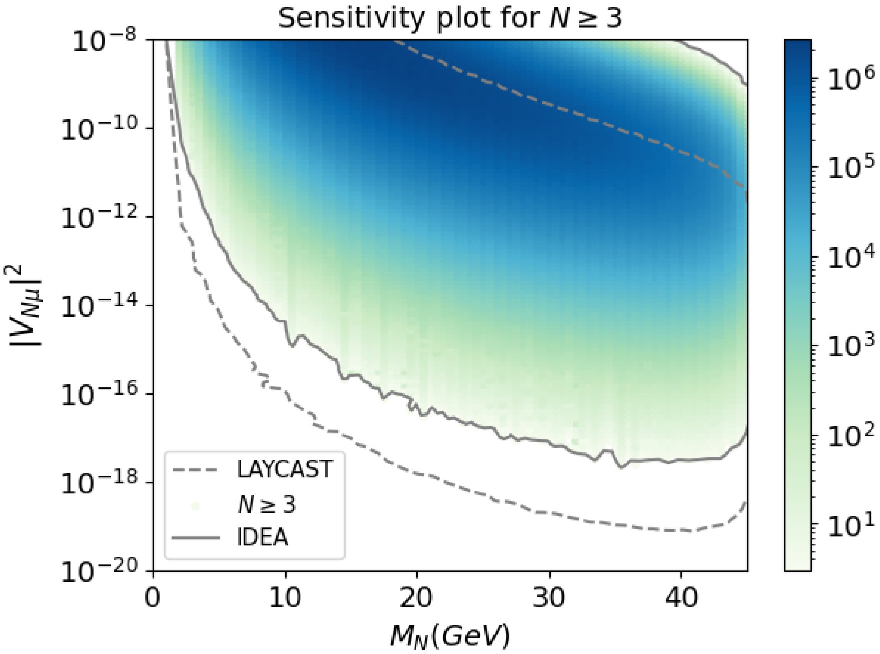

Figure 4.5: Sensitivity plot for $N \geq 3$ at the 95%CL for the process $e^+e^- \to Z' \to NN \to \mu\mu jjjj$ with zero background. The sensitivities correspond to different sections of the detector configuration, inside IDEA and in between IDEA and LAYCAST at the FCC-ee (4y runtime). The plot shows the $M_N - |V_{\mu N}|^2$ plane for fixed $M_{Z'} = \sqrt{s} = 91$ GeV. The colorbar shows the number of expected events, N, for the IDEA detector.

In Figure (4.6), the constraint in the $M_N - M_{Z'}$ shrank to cover only low M_N values of up to 20 GeV, expected for a higher reach on particles with larger decay lengths, and in general the sensitivity curve turned out covering a complementary smaller parameter space for the LAYCAST configuration than the IDEA one. The reason is that in the probabilities calculated for LAYCAST the fiducial volume was considered as starting from the end of IDEA, ie. 5m, which results in a constraint that is exclusive to what the LAYCAST detector can search by itself, and not what both detectors could search together. We also note that the LAYCAST curve is not fully contained by the IDEA one, covering more parameter space (at larger lifetimes) by including a second detector.

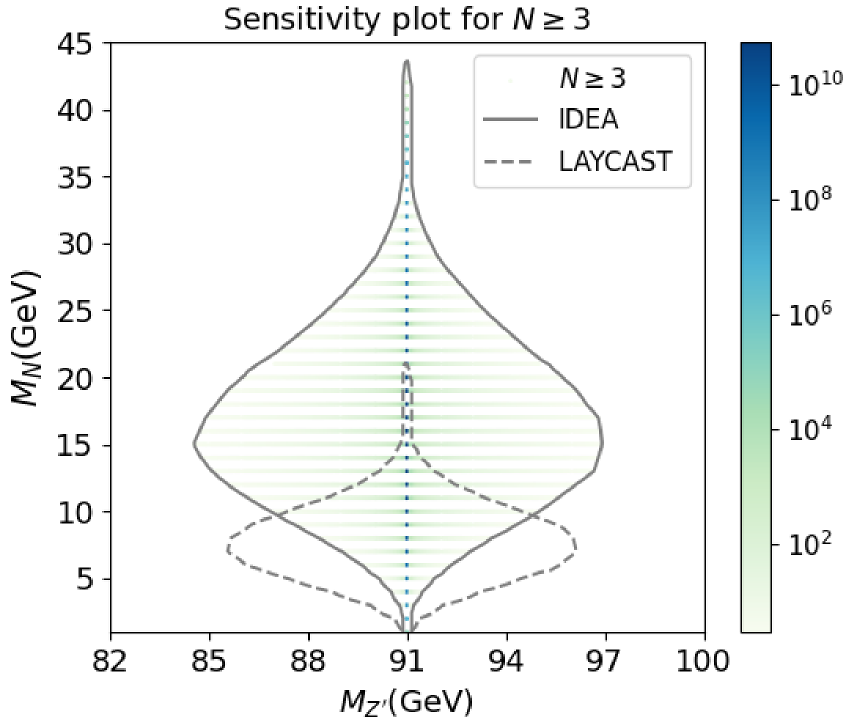

Figure 4.6: Sensitivity plot for $N \geq 3$ at the 95%CL for the process $e^+e^- \to Z' \to NN \to \mu\mu jjjj$ with zero background. The sensitivities correspond to different sections of the detector configuration, inside IDEA and in between IDEA and LAYCAST at the FCC-ee (4y runtime). The plot shows the $M_N - M_{Z'}$ plane for fixed $|V_{lN}|^2 = 10^{-8}$. The colorbar shows the number of expected events, N, for the IDEA detector.

The $M_N - |V_{\mu N}|^2$ mixing plane was simulated only for $g' = 10^{-4}$, as seen in Figures (4.5) and (4.7). The plane is constrained up to the highest M_N kinematically allowed for pair produced HNLs for $\sqrt{s} = M_{Z'} = 91$ GeV, which is 45.5 GeV, and FCC-ee can probe mixings down to 10^{-17} only with the IDEA detector. In Figure (4.6) the sensitivity curve shifts towards lower mixings for a far detector like LAYCAST, since the configuration is sensitive to larger decay lengths. On the other hand, in Figure (4.7) it can be seen that the FCC-ee will already cover an important part of this plane after the first year of runtime.

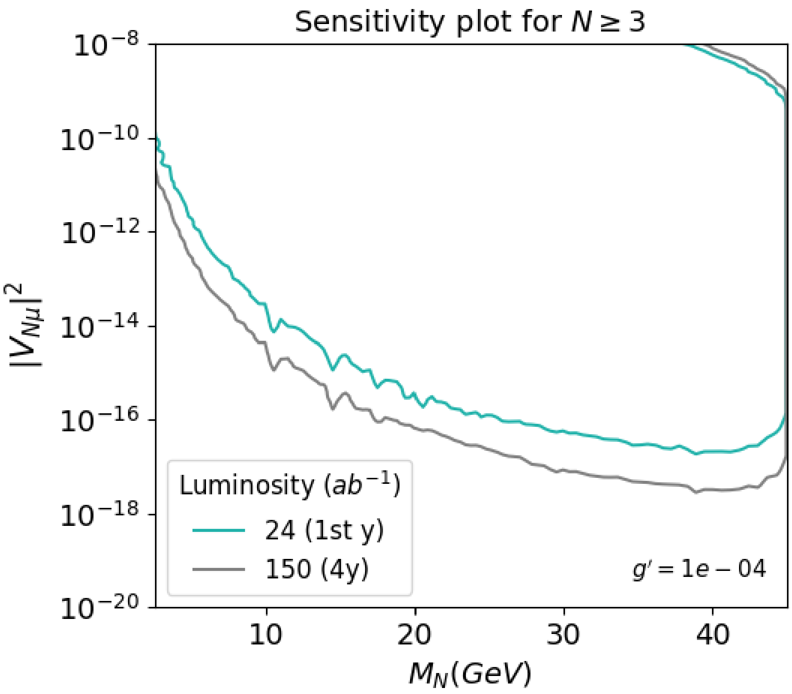

Figure 4.7: Sensitivity plot at the 95%CL for the process $e+e- \rightarrow Z' \rightarrow NN \rightarrow \mu\mu jjjj$, shown on the $M_N - |V_{\mu N}|^2$ plane at the FCC-ee with an IDEA detector, for one and four years runtime.

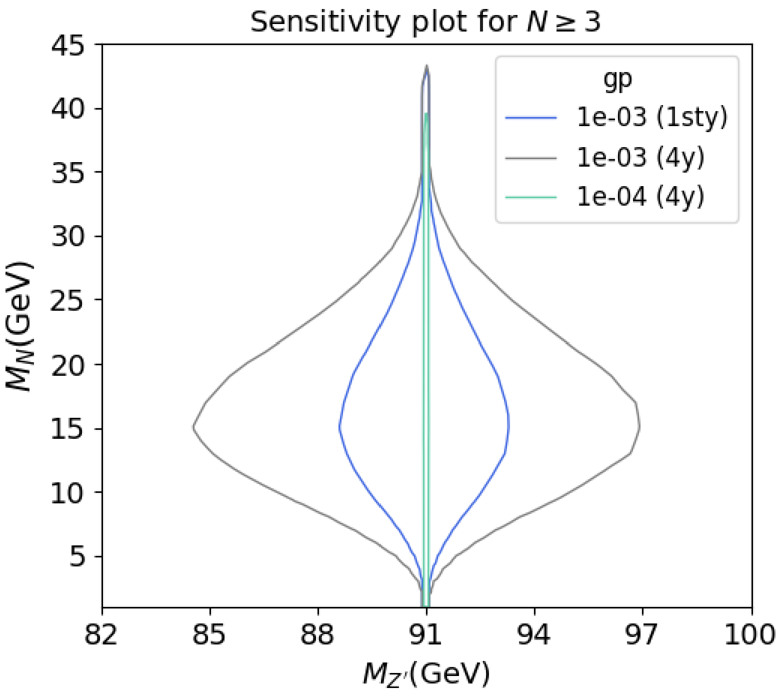

Figure 4.8: Sensitivity plot at the 95%CL for the process $e + e- \to Z' \to NN \to \mu\mu jjjj$ at zero background, shown on the $M_N - M_{Z'}$ plane at the FCC-ee with an IDEA detector, after 1 and 4 years of runtime for $g' = 10^{-3}$ and 10^{-4}.

4.2.1 Discussion

The constraint obtained in the $M_N - |V_{\mu N}|^2$ plane for a long-lived HNL pair produced at the FCC-ee (Fig. (4.5)) is a novel result for the minimal B-L model. Similar curves have been derived for the minimal model at the FCC-ee, as shown in [49], but these focus on HNLs produced from the decay of a Z in the absence of additional gauge symmetries, where pair production is not allowed. In contrast, the B-L model can predict larger cross-sections by including a new gauge boson, Z', allowing the curve to reach lower values of the squared mixing in this plane, which is an interesting LLP search for FCC-ee.

Several observations can be made regarding the sensitivity plots. In Figure (4.5), small mixing values are permitted for HNL masses closer to 45 GeV, since lighter HNLs with small mixing acquire extended lifetimes, reaching decay lengths of the order of hundreds of kilometers and thus decaying very far from the IP, outside of the detector's acceptance. It is also noteworthy that in this plot, the contour is not closed because the highest mass kinematically allowed for pair production is 45.5 GeV, so no mass above this value was simulated. In order to close the constrain, more points will be simulated in future work, but the curve is not expected to go further. On the other hand, in Figure (4.6) one can see that smaller HNL masses around $M_{Z'}/6$ are favored in this scenario. This would be an interesting constraint to impose over the parameter space for calculating a sensitivity plot where the M_N and $M_{Z'}$ masses are not independent parameters. We can see from Figure (3.2) that the cross-section is favored for smaller HNL masses, causing the behavior depicted in Figure (4.6). We note, however, that the probability distribution influences this shape by dictating the horizontal extension of the contour.

As shown in the $c\tau$ plot in Figure (3.7), the smallest squared mixing value for which the HNL can decay inside the IDEA+LAYCAST configuration is 10^{-12}, however, our constraint curve extends to much smaller mixing values, which means HNLs that decay outside of the fiducial volume of the detector. This can be because the efficiency factor, which is the probability function, decreases exponentially at the border of the volume, instead of discontinuously going to zero, as seen in Figures (4.2) and (4.3), therefore for a high enough value of the cross-section and the luminosity, the number of expected events results in $\mathcal{N} > 3$, and the sensitivity plot gets a sort of geometric "illusion acceptance". This issue can be taken into account by imposing by hand that the probability is exactly zero outside of the fiducial volume, which means dropping all events where the HNL has a decay length that misses the volume of the detector. The sensitivity plot under such a constraint was preliminarily calculated and showed to reduce the acceptance in squared mixing by an order of magnitude in Figure (4.5). These effects were not included in the sensitivity plots shown in this thesis, Figures (4.7) and (4.5), due to a lack of statistics with the available simulated data, but are to be considered in future work. Another detail to consider is the cases in which the tangent of θ equals zero, where the distances diverge. Since its expected that only very few events reach the exact value of 0° in θ, and analogously for 180°, as can be noted in the η distribution in Fig.(3.11), this is only expected to help on reducing statistical fluctuations around the contour curve.

It is relevant to note that the plot in Fig. 2 of Ref. [49] shows that within the next two decades, following the planned upgrades and data collection, the HL-LHC could probe through hadronic searches a part of the $M_N - |V_{\mu N}|^2$ plane that we simulated in this work. However the electron-positron search including a far detector increases the sensitivity for M_N values between 1 GeV and 10 GeV. Experiments like ATLAS have searched for M_N values between 5 GeV and 10 GeV, excluding squared mixings greater than 10^{-7} [30]. In our analysis, FCC-ee with a far detector like LAYCAST is sensitive down to approximately $|V_{\mu N}|^2 = 10^{-19}$ for $M_{Z'}$ in a 10 GeV range around the resonance $\sqrt{s} = M_{Z'}$. This shows the IDEA+LAYCAST configuration at the FCC-ee has significant potential for discovering long lived HNLs, with particular improvements in the lighter HNL parameter space in comparison with the HL-LHC, and its noteworthy that IDEA by itself can probe mixings down to 10^{-17}.

4.3 Fast Simulation-Based Analysis for the IDEA Detector

Up until this section, Pythia (along with Python) was used to simulate the acceptance of the IDEA detector to the HNLs in our simulation. This approach primarily accounts for the geometry of the detection, as seen in equation (4.3), but it assumes an ideal detector. In order to simulate the detector response to the particles interactions with it we used `Delphes 3.5.0` [46], which takes as an input the particle-level generated process in `.lhe` files given by a Monte Carlo software like MadGraph, and give as output an object from the ROOT framework which includes all the generated and recollected data, referred to as a Tree [50]. We note that Pythia is installed within Delphes so the parton shower and hadronization are still handled correctly.

Delphes is a faster alternative to full-detector simulation, very useful for approaches that do not require a detailed description of the interactions with the different detector materials, since it performs fast simulations with effective responses. However, this software is capable of providing accurate simulations that account for pile-up and particle flow. [2]

Delphes simulates, by response functions, a tracking system in a solenoidal magnetic field, a calorimeter and a muon system.

The MC generated events are filtered and stored in different ROOT branches, with each branch representing the data for a particular detector element that successfully passed the relevant classification criteria, in concordance with the intrinsic properties of the particles and with the definition of each detector model. Therefore, for example, the tracker branch will filter-out non-charged particles, but also charged particles that fall outside of the detectors acceptance, considering geometrical aspects like decay length, pseudorapidity (η), among others. We note that each class (stored in a ROOT branch) includes functions to access the different kinematic variables. For an example of the available classes and functions see ref. [51]. Along with the MC generated `.lhe` file, each particular detector configuration has to be provided to Delphes in the form of a card, contained in a `.tcl` file. This file details the different detector sections, their respective efficiencies and how the data will be handled in each.

As mentioned, Delphes allows the user to access the generated kinematic information for all the particles involved in the process. In this discussion we will only show results on

---

[2] In hadron-hadron collisions, the overlap of simultaneous events (or pile-up) is produced because hadrons are collided as bunches of particles. In electron-positron experiments the collisions happen one to one, as easier for lighter particles, therefore pile-up can become relevant only in high luminosity experiments like FCC-ee.

kinematic distributions for the tracker branch, leaving kinematic cuts and vertex criteria for future work. In Delphes, the tracking efficiencies are only approximate and are described by an efficiency equation that depends on the magnitude of energy and η. The tracking treats all leptons and hadrons equally, and smearing is performed using a covariance matrix validated with full simulation [46].

The MC generated events for the process $e^+e^- \to Z' \to NN \to \mu\mu jjjj$ in the benchmark $\sqrt{s} = M_{Z'} = 91$ GeV, $M_N = 35$ GeV, $|V_{\mu N}|^2 = 10^{-9}$, $g' = 10^{-4}$ were given to Delphes software along with the respective card for the IDEA detector model. In Figures (4.9(a)) and (4.9(b)), a non normalized distribution for the transverse momenta p_T and the pseudorapidity, η, of the HNL produced muons[3] are plotted along with the distributions for the MC generated muons (which also come from an HNL) as given by MadGraph (i.e. with a detector efficiency of 1), with the purpose of illustrating the effect of the efficiency of the detector.

Since tracks follow an helix path, sometimes they can get closer to the IP after being produced, before moving away. The observable that describes this phenomena and help us to classify displaced activity is the impact parameter. This parameter is the shortest distance between a track and the IP, projected to the transverse plane (d_0) and to the longitudinal plane (d_z). The explicit form of the impact parameter projected into the transverse plane is [20]

$$d_0 = \sqrt{x_d^2 + y_d^2} \sin \phi_m - \phi_d, \tag{4.10}$$

as a function of the daughter coordinates, x_d, y_d and ϕ_d, and the (long lived, in our case) mother coordinate ϕ_m. Since this variables are of major importance when studying long lived particles, we also included plots for the impact parameter d_0 and its projection along the z axis, d_z, which were provided by Delphes, as established in the IDEA card.

---

[3] The tracks were classified as HNL produced muons using the Delphes functions: `.Particle()`, which is a reference to the MC generated particle that corresponds to the selected track, `.M1()`, which gives back the event index of the generated paricle's mother and `.PID()` which gives the mother's ID.

According to the benchmark of the plots shown in Figure (4.9), the decay length of the HNLs that produced the analyzed tracks was 1 cm, this number agrees with the distributions shown for d_0 and d_z of the muons, which peak at that value. This outcome aligns with expectations, as the method described earlier ensured that these tracks originate from the HNL

The efficiency for the reconstruction for MC generated muons, to muon-type tracks, is calculated as $\epsilon = N_{\mu-track}$/N, where N and $N_{\mu-track}$ are the amount of MC simulated events before and after implementing the tracking criteria of the IDEA detector (through Delphes). For the plots in Figures (4.9(a)) and (4.9(b)), $N_{MC} = 199984$, as expected for 100k MC simulated events with two HNLs decaying into one muon (and two jets) per event. The 16 missing HNLs are associated to software error. On the other hand, the amount of events that contain two muon type tracks (produced by an HNL) that passed the tracker criteria of the IDEA detector (implemented through Delphes) is $N_{\mu-track} = 62551$. Therefore the efficiency for this preliminary analysis is $\epsilon = 0.313$. Based on this efficiency, it can be inferred that 30% of the events that contained two final-state muons originating from a pair of HNLs, satisfy the track selection criteria of the IDEA detector, as specified in the IDEA card.

ATLAS and CMS have conducted long lived HNL searches with different criteria depending on the respective production mode and thus on the energy scale: Displaced dilepton searches with no explicit no vertex requirement (CMS), Displaced dilepton vertex search (CMS), Displaced lepton + hadrons vertex search (ATLAS), Displaced dilepton vertex search (ATLAS) or DVs in muon spectrometer (ATLAS). For a brief description of each and further references, see [52]. One can revisit these searches ans recast them to other models, like the search for long lived neutralinos is often reinterpreted for HNL studies as well, see ref. [53].

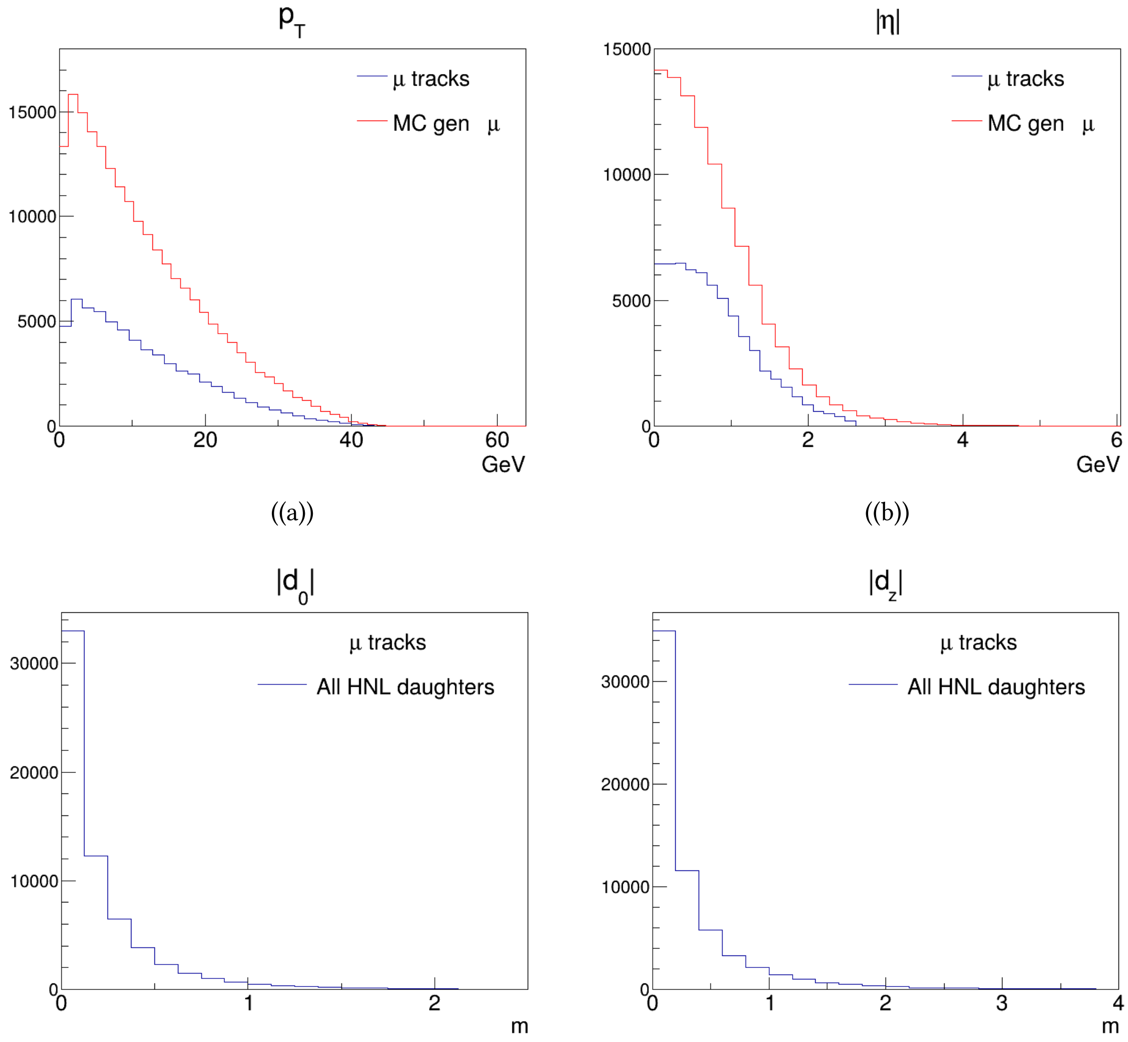

((a)) ((b))

((c)) ((d))

Figure 4.9: Recollected muon type tracks for the IDEA detector simulation at the FCC-ee for the process $e^+e^- \to Z' \to NN \to \mu\mu jjjj$ simulated with `Delphes 3.5.0`, in the benchmark $\sqrt{s} = M_{Z'} = 91$ GeV, $M_N = 35$ GeV, $|V_{\mu N}|^2 = 10^{-9}$, $g' = 10^{-4}$. Figures (a) and (b) show the p_T and $|\eta|$ distributions for muons resulting from an HNL decay, stored in the reconstructed tracks (despicted in blue), and stored in the MC generated events with a detector efficiency of 100% (despicted in red). Figures (c) and (d) show d_0 and d_z for reconstructed tracks which are classified as HNL produced muons.

In future work, a specific search for final-state leptons and at least one displaced vertex at the GeV scale at the FCC-ee will be proposed by estimating the efficiency of the detector's response and performing kinematic cuts on the events given by Delphes. Cuts similar to the ones applied in [54] and [20] for the pair production of an HNL with a mass under 100 GeV decaying into a lepton and two jets will be used as a guide for event selection. The general cuts over the lepton tracks for two displaced vertices are over p_T, η and d_0. Low p_T lepton tracks are excluded for avoiding background and noise from side processes like low energy hadronic or photonic decays, η cuts are a standard constraint imposed to account for the acceptance of the detector, arising from limitations inherent in the detector's geometry, and d_0 larger than ~ 1mm classifies tracks as displaced.

Chapter 5

Conclusion

In this work, the MadGraph MC simulator was used to generate the process $e^+e^- \to Z' \to NN \to \mu\mu jjjj$ in a minimal B-L model with only one HNL, $N = N_2$, which mixes with only one SM neutrino flavour through the mixing element $V_{\mu N}$. Cross sections of the order of 10^2 pb and 10^{-2} pb were obtained for $g' = 10^{-3}$ and 10^{-4} respectively for $\sqrt{s} = M_{Z'}$.

The geometry of one of the prompt detectors proposed by the FCC collaboration, the IDEA detector, was modeled for calculating the probability for an HNL to decay inside of its fiducial volume. This calculation was repeated for the scenery where there's a far detector surrounding IDEA, and the far detector model used is a proposal denominated LAYCAST. We used Pythia 8 and Python 3 to obtain the HNL kinematic information of each MC event, and with it we calculated the probability for it to decay inside IDEA and, separately, inside LAYCAST (outside of IDEA).

With respect to the probability distributions, they were calculated for the Vertex Finder in the IDEA detector and for the fiducial volume that starts at the external border of IDEA and ends in the LAYCAST trackers in the cavern. These distributions peaked within the corresponding fiducial volumes. Since the ϕ distribution of the HNLs is uniform (Figure

(3.11)), the loss of HNLs through the cavern floor for LAYCAST does not have a big impact beyond introducing statistical uncertainty by reducing the amount of events that contribute to the mean probability by giving a nonzero value. If the process is symmetrical around the azimuthal angle for every benchmark, then the decrease in statistics will be constant. On the appendix of the LAYCAST ref. [49], a study on how the election of the position of the IP, including an analyses on the lack of tracker floor, is done, resulting in minor effects overall.

The probability is an efficiency factor used to calculate the number of expected events and with it a sensitivity constrain was obtained for both the $M_N - M_{Z'}$ and the $M_N - |V_{\mu N}|^2$ planes. Both of the studied planes show that in the $\sqrt{s} = M_{Z'}$ resonance, FCC-ee with an IDEA detector is sensitive to all HNL masses between 1 GeV and 45 GeV, starting from the first year of runtime, for both $g' = 10^{-3}$ and $g' = 10^{-4}$.

We note that the sensitivity analysis in the $M_N - M_{Z'}$ was conducted for two values of g', 10^{-3} and 10^{-4}, but the DarkCast plot in ref. [32] shows using experimental searches that $g' = 10^{-3}$ is right at the exclusion border defined by the existing experimental searches, and given the resulting sensitivity for $g' = 10^{-4}$, the $M_N - M_{Z'}$ plane is not interesting on a sector of the parameter space that is safely free from current constrains. On the other hand and for the same reason, the $M_N - |V_{\mu N}|^2$ plane was only simulated for $g' = 10^{-4}$. Our search was not found in the literature for the minimal B-L model at the FCC-ee, making this a novel study, with sensitivities down to 10^{-18} in mixing for an IDEA-like prompt detector after 4 y runtime.

To follow up on this work, an algorithm for identifying, selecting, and filtering displaced vertices will be developed using Delphes, with the purpose of obtaining sensitivity prospects that account for the detector's response to particle's interactions. It would be interesting to get in touch with the LAYCAST authors to check if they can provide a Delphes card for their proposed detector and include it in our analyses. Since LAYCAST is just one tracker layer, time could be invested in creating a toy card for a tracker open box that simulates the

LAYCAST detector with efficiencies similar to the IDEA ones.

In this work, as a first approach to calculating an efficiency factor that takes into account the detector components response to the passage of the simulated particles, we compared the kinematical variables of the events stored in the "Tracker" branch of the ROOT tree with the ones of the MC generated data that have a detector efficiency of 1. For muons produced from the decay of an HNL, the efficiency of the reconstruction considering only the tracking selection criteria provided in the IDEA card is $\epsilon = 0.313$.

It is relevant to note that Delphes also offers reconstructed events in a module exclusive for muons. These events undergo additional cuts compared to those stored in the 'Tracker' branch by effectively simulating the muon system, and thus the number of MC events is reduced by at least two orders of magnitude by passing these cuts, which makes a muon-system level study interesting but less effective computationally.

This work can also be thoroughly complemented by extending the simulated parameter space. Heavier Z' masses can be analyzed for other running stages of the FCC-ee with smaller luminosities. As our cross section plot shows for a Higgs scale Z' boson, the value of the cross section is not suppressed for a pair produced HNL with a mass of 5GeV and $|V_{\mu N}|^2 = 10^{-8}$, which would behave as an LLP. Therefore it is to be expected that IDEA at the FCC-ee can search this sector as well with enough sensitivity, considering $\mathcal{L} = 50$ ab^{-1} after four years of runtime in Higgs Factory mode. The prospects obtained in this work would be very interesting to analyze in the $U(1)_X$ model, since, as it was mentioned in the introduction, the cross sections are higher due to the more general quantum number, thus more sensitive searches can be proposed.

In conclusion, this work proposes a search strategy for the Future Circular Collider at the Electron-Positron mode (FCC-ee) to probe long-lived Heavy Neutral Leptons (HNLs) within an unconstrained and experimentally accessible parameter space. By utilizing the IDEA detector, this study presents sensitivity prospects that highlight the potential of FCC-ee in detecting these particles. This approach not only contributes to the exploration of beyond the Standard Model physics but also underscores the importance of advancing experimental techniques to search for long-lived particles at upcoming collider experiments.

Appendix A

Appendix

A.1 Relevant Feynmann rules for HNLs

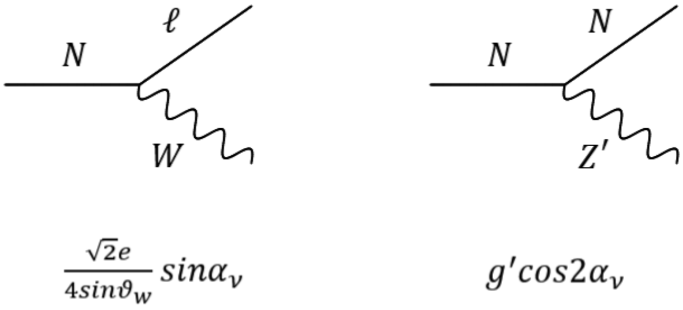

Figure A.1: Feynmann rules involving HNLs in our simulated process. [42]

A.2 Field Content of the B-L Model

Fields	Field Content	$SU(3)_C$	$SU(2)_L$	$U(1)_Y$	$U(1)_{B-L}$
g_μ^α	g_μ^α	8	1	1	0
$W^{\mu a}$	W_μ^a	1	3	0	1
B^μ	B^μ	1	1	0	0
B'^μ	B'^μ	1	1	0	0
L_i	$L_i = \begin{pmatrix} N_{L_i} \\ e_{L_i} \end{pmatrix}$	1	2	1/2	-1
e_{Ri}	e_{Ri}	1	1	-1	-1
N_{Ri}	N_{Ri}	1	1	0	-1
Q_i	$\begin{pmatrix} u_{L_i} \\ d_{L_i} \end{pmatrix}$	3	2	1/6	1/3
d_{Li}^c	u_{R_i}	3	1	1/3	1/3
u_{Li}^c	u_{R_i}	3	1	-1/3	1/3
H	$\begin{pmatrix} H^+ \\ H^0 \end{pmatrix}$	1	2	-1/2	0
χ	χ	1	1	0	2

Table A.1: Standard Model extended with the non minimal B-L symmetry of particle physics. $i = 1, ..., 3$ are generation indices, $a = 1, ..., 3$ for W and $\alpha = 1, ..., 8$ for the gluons.

A.3 Boost factor and decay length projected to the z axis

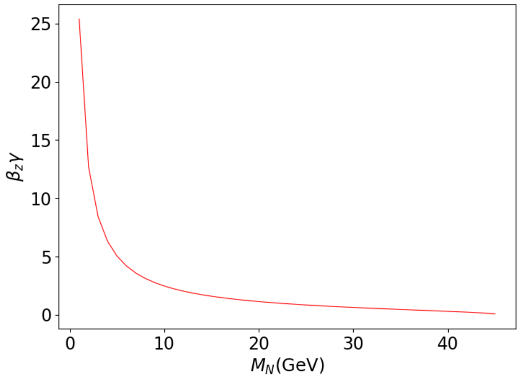

Figure A.2: Boost factor projected to the z axis.

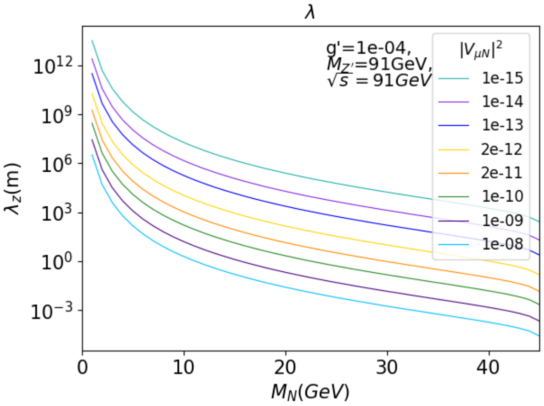

Figure A.3: Decay length projected to the z axis, calculated with the method previously described in Chapter 3.

A.4 Benchmark Table

M_N (GeV)	$\lvert V_{\tau N}\rvert^2$	$\sqrt{s}$ (GeV)	$M_{Z'}$ (GeV)	BR($N \to \mu jj$)	σ_1 (pb)	σ_2 (pb)	eff	Γ (GeV)	$c\tau$ (m)	g'	$\mathcal{L}$ (ab^{-1})	N
20	1×10^{-12}	91	91	0.514	451.93	232.544	0.0055817	1.553546×10^{-18}	127.08	1×10^{-3}	1.5×10^{8}	1.9×10^{8}
30	1×10^{-14}	91	91	0.507	265.04	134.567	0.0007	7.483732×10^{-20}	2638.12	1×10^{-3}	1.5×10^{8}	1.4×10^{7}
20	1×10^{-12}	91	91	0.514	0.04519	0.0232544	0.0055817	1.553546×10^{-18}	127.08	1×10^{-4}	1.5×10^{8}	1.9×10^{4}
30	1×10^{-14}	91	91	0.507	0.0265	0.0134567	0.0007	7.4837×10^{-20}	2638.133	1×10^{-4}	1.5×10^{8}	1.4152×10^{5}

Table A.2: Two benchmarks for our calculation of the number of expected events. $\sigma_1 = \sigma(e^+e^- \to Z' \to NN)$ and $\sigma_2 = \sigma(e^+e^- \to Z' \to NN \to \mu\mu jjjj)$. In this case, eff=$\langle P(\theta)\rangle$ is the probability of decay inside the fiducial volume. Note that this table is originally 5x12; it was divided in half to accommodate space.

Bibliography

[1] e. a. Aghanim N., “Planck2018 results: Vi. cosmological parameters,” *Astronomy amp; Astrophysics*, vol. 641, A6, Sep. 2020, ISSN: 1432-0746. DOI: 10.1051/0004-6361/201833910. [Online]. Available: http://dx.doi.org/10.1051/0004-6361/201833910.

[2] M. Peskin and D. Schroeder, *An Introduction To Quantum Field Theory* (Frontiers in Physics). Avalon Publishing, 1995, ISBN: 9780813345437. [Online]. Available: https://books.google.cl/books?id=EVeNNcslvX0C.

[3] G. Aad and e. a. Abajyan, “Observation of a new particle in the search for the standard model higgs boson with the atlas detector at the lhc,” *Physics Letters B*, vol. 716, no. 1, 1–29, Sep. 2012, ISSN: 0370-2693. DOI: 10.1016/j.physletb.2012.08.020. [Online]. Available: http://dx.doi.org/10.1016/j.physletb.2012.08.020.

[4] A. P. Heinson and T. M. Liss, “Top quark mass measurements,” in *AIP Conference Proceedings*, vol. 870, AIP, 2006, 223–227. DOI: 10.1063/1.2402623. [Online]. Available: http://dx.doi.org/10.1063/1.2402623.

[5] T. L. C. T. O. C. T. S. C. T. L. E. W. G. T. S. E. The ALEPH Collaboration The DELPHI Collaboration and H. F. Groups, “Precision electroweak measurements on the z resonance,” *Physics Reports*, vol. 427, no. 5, pp. 257–454, 2006, ISSN: 0370-1573. DOI: https://doi.org/10.1016/j.physrep.2005.12.006. [Online]. Available: https://www.sciencedirect.com/science/article/pii/S0370157305005119.

[6] A. Collaboration *et al.*, *Precision electroweak measurements and constraints on the standard model*, 2011. arXiv: 1012.2367 `[hep-ex]`. [Online]. Available: https://arxiv.org/abs/1012.2367.

[7] R. Davis, D. S. Harmer, and K. C. Hoffman, "Search for neutrinos from the sun," *Phys. Rev. Lett.*, vol. 20, pp. 1205–1209, 21 1968. DOI: 10.1103/PhysRevLett.20.1205. [Online]. Available: https://link.aps.org/doi/10.1103/PhysRevLett.20.1205.

[8] e. a. Fukuda Y., "Solar neutrino data covering solar cycle 22," *Phys. Rev. Lett.*, vol. 77, pp. 1683–1686, 9 1996. DOI: 10.1103/PhysRevLett.77.1683. [Online]. Available: https://link.aps.org/doi/10.1103/PhysRevLett.77.1683.

[9] e. a. Fukuda Y., "Measurement of the solar neutrino energy spectrum using neutrino-electron scattering," *Phys. Rev. Lett.*, vol. 82, pp. 2430–2434, 12 1999. DOI: 10.1103/PhysRevLett.82.2430. [Online]. Available: https://link.aps.org/doi/10.1103/PhysRevLett.82.2430.

[10] e. a. Fukuda Y., "Evidence for oscillation of atmospheric neutrinos," *Phys. Rev. Lett.*, vol. 81, pp. 1562–1567, 8 1998. DOI: 10.1103/PhysRevLett.81.1562. [Online]. Available: https://link.aps.org/doi/10.1103/PhysRevLett.81.1562.

[11] e. a. Eguchi K., "First results from kamland: Evidence for reactor antineutrino disappearance," *Phys. Rev. Lett.*, vol. 90, p. 021 802, 2 2003. DOI: 10.1103/PhysRevLett.90.021802. [Online]. Available: https://link.aps.org/doi/10.1103/PhysRevLett.90.021802.

[12] P. Minkowski, "$\mu \to e\gamma$ at a rate of one out of 109 muon decays?" *Physics Letters B*, vol. 67, no. 4, pp. 421–428, 1977, ISSN: 0370-2693. DOI: https://doi.org/10.1016/0370-2693(77)90435-X. [Online]. Available: https://www.sciencedirect.com/science/article/pii/037026937790435X.

[13] M. e. a. Aker, "Improved upper limit on the neutrino mass from a direct kinematic method by katrin," *Physical Review Letters*, vol. 123, no. 22, Nov. 2019, ISSN: 1079-7114.

DOI: 10.1103/physrevlett.123.221802. [Online]. Available: http://dx.doi.org/10.1103/PhysRevLett.123.221802.

[14] e. a. Alimena Juliette, "Searching for long-lived particles beyond the standard model at the large hadron collider," *Journal of Physics G: Nuclear and Particle Physics*, vol. 47, no. 9, p. 090 501, Sep. 2020, ISSN: 1361-6471. DOI: 10.1088/1361-6471/ab4574. [Online]. Available: http://dx.doi.org/10.1088/1361-6471/ab4574.

[15] e. a. Curtin, "Long-lived particles at the energy frontier: The mathusla physics case," *Reports on Progress in Physics*, vol. 82, no. 11, p. 116 201, Oct. 2019, ISSN: 1361-6633. DOI: 10.1088/1361-6633/ab28d6. [Online]. Available: http://dx.doi.org/10.1088/1361-6633/ab28d6.

[16] A. M. Sirunyan, A. Tumasyan, W. Adam, F. Ambrogi, E. Asilar, and e. a. Bergauer, "Search for disappearing tracks as a signature of new long-lived particles in proton-proton collisions at $\sqrt{s} = 13$ tev," *Journal of High Energy Physics*, vol. 2018, no. 8, Aug. 2018, ISSN: 1029-8479. DOI: 10.1007/jhep08(2018)016. [Online]. Available: http://dx.doi.org/10.1007/JHEP08(2018)016.

[17] A. e. a. Sirunyan, "Search for disappearing tracks in proton-proton collisions at $\sqrt{s} = 13TeV$," *Physics Letters B*, vol. 806, p. 135 502, Jul. 2020, ISSN: 0370-2693. DOI: 10.1016/j.physletb.2020.135502. [Online]. Available: http://dx.doi.org/10.1016/j.physletb.2020.135502.

[18] G. Aad, B. Abbott, D. C. Abbott, and e. a. Abdinov, "Search for heavy neutral leptons in decays of w bosons produced in 13 tev pp collisions using prompt and displaced signatures with the atlas detector," *Journal of High Energy Physics*, vol. 2019, no. 10, Oct. 2019, ISSN: 1029-8479. DOI: 10.1007/jhep10(2019)265. [Online]. Available: http://dx.doi.org/10.1007/JHEP10(2019)265.

[19] L. Basso, A. Belyaev, S. Moretti, and C. H. Shepherd-Themistocleous, "Phenomenology of the minimal b-l extension of the standard model: Z' and neutrinos," *Physical*

Review D, vol. 80, no. 5, Sep. 2009, ISSN: 1550-2368. DOI: 10.1103/physrevd.80.055030. [Online]. Available: http://dx.doi.org/10.1103/PhysRevD.80.055030.

[20] C.-W. Chiang, G. Cottin, A. Das, and S. Mandal, "Displaced heavy neutrinos from z decays at the lhc," *Journal of High Energy Physics*, vol. 2019, no. 12, Dec. 2019, ISSN: 1029-8479. DOI: 10.1007/jhep12(2019)070. [Online]. Available: http://dx.doi.org/10.1007/JHEP12(2019)070.

[21] T. Appelquist, B. A. Dobrescu, and A. R. Hopper, "Nonexotic neutral gauge bosons," *Physical Review D*, vol. 68, no. 3, Aug. 2003, ISSN: 1089-4918. DOI: 10.1103/physrevd.68.035012. [Online]. Available: http://dx.doi.org/10.1103/PhysRevD.68.035012.

[22] C. Collaboration, *The Future Circular Collider*. [Online]. Available: https://home.cern/science/accelerators/future-circular-collider.

[23] E. S. for Particle Physics (ESPP), "The European Strategy for Particle Physics Update 2013. La stratégie européenne pour la physique des particules Mise à jour 2013. 16th Session of European Strategy Council," *https://cds.cern.ch/record/1567258*, 2013.

[24] E. S. for Particle Physics (ESPP), "The European Strategy for Particle Physics Update 2020.," *https://cds.cern.ch/record/1567279*, 2020.

[25] A. Abada *et al.*, "FCC-ee: The Lepton Collider: Future Circular Collider Conceptual Design Report Volume 2," *Eur. Phys. J. ST*, vol. 228, no. 2, pp. 261–623, 2019. DOI: 10.1140/epjst/e2019-900045-4.

[26] J. Pekkanen, "Allegro fcc-ee detector concept noble liquid calorimetry," *Nuclear Instruments and Methods in Physics Research Section A: Accelerators, Spectrometers, Detectors and Associated Equipment*, vol. 1069, p. 169 921, 2024, ISSN: 0168-9002. DOI: https://doi.org/10.1016/j.nima.2024.169921. [Online]. Available: https://www.sciencedirect.com/science/article/pii/S0168900224008477.

[27] M. Chrząszcz, M. Drewes, and J. Hajer, "Hecate: A long-lived particle detector concept for the fcc-ee or cepc," *The European Physical Journal C*, vol. 81, no. 6, Jun. 2021, ISSN: 1434-6052. DOI: 10.1140/epjc/s10052-021-09253-y. [Online]. Available: http://dx.doi.org/10.1140/epjc/s10052-021-09253-y.

[28] Y. Lu, Y. nan Mao, K. Wang, and Z. S. Wang, *Laycast: Layered cavern surface tracker at future electron-positron colliders*, 2024. arXiv: 2406.05770 [hep-ph]. [Online]. Available: https://arxiv.org/abs/2406.05770.

[29] T. C. S. Group, *Cepc conceptual design report: Volume 2 - physics detector*, 2018. arXiv: 1811.10545 [hep-ex]. [Online]. Available: https://arxiv.org/abs/1811.10545.

[30] E. Fernández-Martínez, M. González-López, J. Hernández-García, M. Hostert, and J. López-Pavón, "Effective portals to heavy neutral leptons," *Journal of High Energy Physics*, vol. 2023, no. 9, Sep. 2023, ISSN: 1029-8479. DOI: 10.1007/jhep09(2023)001. [Online]. Available: http://dx.doi.org/10.1007/JHEP09(2023)001.

[31] A. Das, P. B. Dev, and N. Okada, "Long-lived tev-scale right-handed neutrino production at the lhc in gauged u(1) model," *Physics Letters B*, vol. 799, p. 135 052, Dec. 2019, ISSN: 0370-2693. DOI: 10.1016/j.physletb.2019.135052. [Online]. Available: http://dx.doi.org/10.1016/j.physletb.2019.135052.

[32] F. F. Deppisch, S. Kulkarni, and W. Liu, "Heavy neutrino production via z' at the lifetime frontier," *Physical Review D*, vol. 100, no. 3, Aug. 2019, ISSN: 2470-0029. DOI: 10.1103/physrevd.100.035005. [Online]. Available: http://dx.doi.org/10.1103/PhysRevD.100.035005.

[33] A. Das, S. Mandal, T. Nomura, and S. Shil, "Heavy majorana neutrino pair production from z' at hadron and lepton colliders," *Physical Review D*, vol. 105, no. 9, May 2022, ISSN: 2470-0029. DOI: 10.1103/physrevd.105.095031. [Online]. Available: http://dx.doi.org/10.1103/PhysRevD.105.095031.

[34] S. Amrith, J. M. Butterworth, F. F. Deppisch, W. Liu, A. Varma, and D. Yallup, "Lhc constraints on a b l gauge model using contur," *Journal of High Energy Physics*, vol. 2019, no. 5, May 2019, ISSN: 1029-8479. DOI: 10.1007/jhep05(2019)154. [Online]. Available: http://dx.doi.org/10.1007/JHEP05(2019)154.

[35] J. Butterworth, "Bsm constraints from model-independent measurements: A contur update," *Journal of Physics: Conference Series*, vol. 1271, p. 012 013, Jul. 2019. DOI: 10.1088/1742-6596/1271/1/012013.

[36] K. Bondarenko, A. Boyarsky, D. Gorbunov, and O. Ruchayskiy, "Phenomenology of gev-scale heavy neutral leptons," *Journal of High Energy Physics*, vol. 2018, no. 11, Nov. 2018, ISSN: 1029-8479. DOI: 10.1007/jhep11(2018)032. [Online]. Available: http://dx.doi.org/10.1007/JHEP11(2018)032.

[37] A. M. Sirunyan and A. e. a. Tumasyan, "Search for high-mass resonances in dilepton final states in proton-proton collisions at $\sqrt{s} = 13$ tev," *Journal of High Energy Physics*, vol. 2018, no. 6, Jun. 2018, ISSN: 1029-8479. DOI: 10.1007/jhep06(2018)120. [Online]. Available: http://dx.doi.org/10.1007/JHEP06(2018)120.

[38] K. A. Urquía-Calderón, "Long-lived heavy neutral leptons at lepton colliders as a probe of left-right-symmetric models," *Physical Review D*, vol. 109, no. 5, Mar. 2024, ISSN: 2470-0029. DOI: 10.1103/physrevd.109.055002. [Online]. Available: http://dx.doi.org/10.1103/PhysRevD.109.055002.

[39] C. B. Verhaaren *et al.*, "Searches for long-lived particles at the future fcc-ee," *Frontiers in Physics*, vol. 10, Sep. 2022, ISSN: 2296-424X. DOI: 10.3389/fphy.2022.967881. [Online]. Available: http://dx.doi.org/10.3389/fphy.2022.967881.

[40] J. Alwall *et al.*, "The automated computation of tree-level and next-to-leading order differential cross sections, and their matching to parton shower simulations," *Journal*

of High Energy Physics, vol. 2014, no. 7, 2014, ISSN: 1029-8479. DOI: 10.1007/jhep07(2014)079. [Online]. Available: http://dx.doi.org/10.1007/JHEP07(2014)079.

[41] C. Bierlich *et al.*, *A comprehensive guide to the physics and usage of pythia 8.3*, 2022. arXiv: 2203.11601 `[hep-ph]`. [Online]. Available: https://arxiv.org/abs/2203.11601.

[42] L. Basso, *Phenomenology of the minimal b-l extension of the standard model at the lhc*, 2011. arXiv: 1106.4462 `[hep-ph]`. [Online]. Available: https://arxiv.org/abs/1106.4462.

[43] C. Degrande, C. Duhr, B. Fuks, D. Grellscheid, O. Mattelaer, and T. Reiter, "Ufo – the universal feynrules output," *Computer Physics Communications*, vol. 183, no. 6, 1201–1214, Jun. 2012, ISSN: 0010-4655. DOI: 10.1016/j.cpc.2012.01.022. [Online]. Available: http://dx.doi.org/10.1016/j.cpc.2012.01.022.

[44] P. Artoisenet, R. Frederix, O. Mattelaer, and R. Rietkerk, "Automatic spin-entangled decays of heavy resonances in monte carlo simulations," *Journal of High Energy Physics*, vol. 2013, no. 3, Mar. 2013, ISSN: 1029-8479. DOI: 10.1007/jhep03(2013)015. [Online]. Available: http://dx.doi.org/10.1007/JHEP03(2013)015.

[45] e. a. J. M. Butterworth, *The tools and monte carlo working group summary report from the les houches 2009 workshop on tev colliders*, 2010. arXiv: 1003.1643 `[hep-ph]`. [Online]. Available: https://arxiv.org/abs/1003.1643.

[46] J. de Favereau *et al.*, "Delphes 3: A modular framework for fast simulation of a generic collider experiment," *Journal of High Energy Physics*, vol. 2014, no. 2, Feb. 2014, ISSN: 1029-8479. DOI: 10.1007/jhep02(2014)057. [Online]. Available: http://dx.doi.org/10.1007/JHEP02(2014)057.

[47] M. Thomson, *Modern Particle Physics*. Cambridge University Press, 2013.

[48] Z. S. Wang and K. Wang, "Physics with far detectors at future lepton colliders," *Phys. Rev. D*, vol. 101, p. 075 046, 7 2020. DOI: 10.1103/PhysRevD.101.075046. [Online]. Available: https://link.aps.org/doi/10.1103/PhysRevD.101.075046.

[49] W. Liu, S. Kulkarni, and F. F. Deppisch, *Revealing the origin of neutrino masses through displaced shower searches in the cms muon system*, 2024. arXiv: 2407.20676 `[hep-ph]`. [Online]. Available: https://arxiv.org/abs/2407.20676.

[50] R. CERN collaboration, *Root manual.* [Online]. Available: https://root.cern/manual/.

[51] *WorkBook/RootTreeDescription &2013; Delphes — cp3.irmp.ucl.ac.be*, https://cp3.irmp.ucl.ac.be/projects/delphes/wiki/WorkBook/RootTreeDescription, [Accessed 02-01-2025].

[52] B. Batell, M. Pospelov, and B. Shuve, "Shedding light on neutrino masses with dark forces," *Journal of High Energy Physics*, vol. 2016, no. 8, Aug. 2016, ISSN: 1029-8479. DOI: 10.1007/jhep08(2016)052. [Online]. Available: http://dx.doi.org/10.1007/JHEP08(2016)052.

[53] G. Cottin, J. C. Helo, N. A. Neill, F. Hernández-Pinto, and Z. S. Wang, "Searching for light neutralinos with a displaced vertex at the lhc," *Journal of High Energy Physics*, vol. 2022, no. 10, Oct. 2022, ISSN: 1029-8479. DOI: 10.1007/jhep10(2022)095. [Online]. Available: http://dx.doi.org/10.1007/JHEP10(2022)095.

[54] F. F. Deppisch, W. Liu, and M. Mitra, "Long-lived heavy neutrinos from higgs decays," *Journal of High Energy Physics*, vol. 2018, no. 8, Aug. 2018, ISSN: 1029-8479. DOI: 10.1007/jhep08(2018)181. [Online]. Available: http://dx.doi.org/10.1007/JHEP08(2018)181.